The DOI for this manuscript is doi: 10.1175/JPO-D-13-0120.1

The final published version of this manuscript will replace the preliminary version at the above DOI once it is available.

If you would like to cite this EOR in a separate work, please use the following full citation:

Tulloch, R., R. Ferrari, O. Jahn, A. Klocker, J. Lacasce, J. Ledwell, J. Marshall, M. Messias, K. Speer, and A. Watson, 2014: Direct Estimate of Lateral Eddy Diffusivity Upstream of Drake Passage. J. Phys. Oceanogr. doi:10.1175/JPO-D-13-0120.1, in press.

Direct Estimate of Lateral Eddy Diffusivity Upstream of Drake Passage

Ross Tulloch, Raffaele Ferrari,* Oliver Jahn

Department of Earth, Atmospheric and Planetary Sciences, Massachusetts Institute of Technology, Cambridge, MA

Andreas Klocker

Institute for Marine and Antarctic Studies, University of Tasmania, Hobart, Australia

Joseph LaCasce

Department of Geosciences, University of Oslo, Oslo, Norway

James R. Ledwell

Woods Hole Oceanographic Institution, Woods Hole, MA

John Marshall

Department of Earth, Atmospheric and Planetary Sciences, Massachusetts Institute of Technology, Cambridge, MA

MARIE-JOSE MESSIAS

School of Environmental Sciences, University of East Anglia, Norwich, UK

KEVIN SPEER

Department of Earth, Ocean and Atmospheric Science, Florida State University, Tallahassee, Florida

Geophysical Fluid Dynamics Institute, Tallahassee, FL

ANDREW WATSON

School of Environmental Sciences, University of East Anglia, Norwich, UK

* *Corresponding author address:* Raffaele Ferrari, Department of Earth, Atmospheric and Planetary Sciences, Massachusetts Institute of Technology, 77 Massachusetts Avenue, Cambridge MA 02139.

E-mail: rferrari@mit.edu

Abstract

The first direct estimate of the rate at which geostrophic turbulence mixes tracers across the Antarctic Circumpolar Current is presented. The estimate is computed from the spreading of a tracer released upstream of Drake Passage as part of the Diapycnal and Isopycnal Mixing Experiment in the Southern Ocean (DIMES). The meridional eddy diffusivity, a measure of the rate at which the area of the tracer spreads along an isopycnal across the Antarctic Circumpolar Current, is 710±260 m^2s^{-1} at 1500 m depth. The estimate is based on an extrapolation of the tracer based diffusivity using output from numerical tracers released in a $1/20^{th}$ of a degree model simulation of the circulation and turbulence in the Drake Passage region. The model is shown to reproduce the observed spreading rate of the DIMES tracer and suggests that the meridional eddy diffusivity is weak in the upper kilometer of the water column with values below 500 m^2s^{-1} and peaks at the steering level, near 2 km, where the eddy phase speed is equal to the mean flow speed. These vertical variations are not captured by ocean models presently used for climate studies, but they significantly affect the ventilation of different water masses.

1 Introduction

At the latitudes of the Antarctic Circumpolar Current (ACC), waters from the Atlantic, Indian and Pacific Oceans are brought to the surface by the Roaring Forties to be transformed into Subantarctic Mode Waters to the north and Antarctic Bottom Waters to the south (Marshall and Speer, 2012). This global transformation of water masses is achieved by intense air-sea exchange of heat, fresh water, carbon, and other chemical tracers in the Southern Ocean and exerts a strong control on Earth's climate. Above the sill depth of the Drake Passage, the circulation is dominated zonally by the ACC and meridionally by the sum of a wind-driven meridonal overturning circulation (MOC) plus a MOC driven by the turbulent eddies generated through instabilities of the ACC (Johnson and Bryden, 1989; Speer et al., 2000; Marshall and Radko, 2003). The air-sea fluxes and Earth's climate are therefore very sensitive to oceanic turbulence in the Southern Ocean. The current debate as to whether Southern Ocean carbon uptake will increase or decrease in a warming climate stems from different assumptions about the changes in oceanic turbulence (Russell et al., 2006; Abernathey et al., 2011).

Despite its importance for climate studies, there have not been direct observational estimates of the rate of mixing which drives the eddy-induced circulation across the ACC. Indirect estimates have been made, for example, by Stammer (1998) who used scaling laws and the surface geostrophic velocity from altimetry, and by Marshall et al. (2006) who drove numerical tracers by the altimetric velocity field. Phillips and Rintoul (2000) attempted to estimate the fluxes of heat and momentum from mooring data, but not the rate at which tracers are mixed. Here we present the first direct measurements based on the spreading of a tracer deliberately released as part of the Diapycnal and Isopycnal Mixing Experiment in the Southern Ocean (DIMES). The mixing is quantified with an eddy diffusivity, which is defined in terms of the spreading rate of the meridional distribution of the tracer, once it asymptotes a constant. The eddy diffusivity is a tensor $\mathbf{K}$ which quantifies the growth of the patch in all three dimensions. Here we will focus on the component of the diffusivity representing the tracer spreading along neutral density surface (isopycnal mixing) and across the ACC, because this is the component that drives the eddy-induced MOC and plays an important role in setting the strength of both the upper and lower overturning cells in the Southern Ocean.

The goal of this paper is to infer an isopycnal diffusivity based on the lateral dispersion of the anthropogenic tracer released in DIMES. The tracer was released on an isopycnal surface near 1500 meters depth, at the interface between the upper and lower MOC cells, in the Pacific sector of the Southern Ocean 2300 km upstream of the Drake Passage, midway between the Polar Front and the Subantarctic Front. Ledwell et al. (2011) estimated that after one year the tracer spread vertically to a Gaussian profile in density with a standard deviation of less than 30 m relative to the target density surface, and was thus confined to a very thin layer.

Our analysis focuses on the first year of spreading when most of the tracer remained west of the Drake Passage; numerical simulations suggest that the leading edge of the tracer reached the Drake Passage after somewhat less than two years. We focus on measurements collected in the sector upstream of the Drake Passage, because the ACC jets are mainly zonal there. Past the Drake Passage, the jets strongly meander and it is difficult to separate along and across-jet dispersion. Furthermore, the tracer sampling downstream of the Drake Passage may not have been adequate to determine cross-stream isopycnal mixing as it was designed to estimate the diapycnal diffusivity; the tracer was sampled only along the individual transects shown in Fig. 1a with no attempt to map the whole tracer patch.

Due to the temporal and spatial scales involved, measuring isopycnal diffusivity by sampling a tracer spreading through the ocean is difficult, since only a fraction of the tracer distribution can be directly sampled. Some method must be developed to extrapolate the tracer measurements and infer where the unsampled tracer may have spread. Ledwell et al. (1998) estimated the isopycnal diffusivity at the mesoscale in the North Atlantic pycnocline by fitting a two-dimensional Gaussian to the tracer patch measured 30 months after release. Assuming such a 2-D Gaussian is perhaps reasonable in a region with weak mean flows, although even at their site Ledwell et al. (1998) suspected a role played by gyre-scale strain in the mean flow in enhancing the apparent zonal diffusion. The assumption of 2-D Gaussian spreading cannot be used in the Southern Ocean, where the tracer is advected rapidly downstream by the meandering ACC jets, at the same time being dispersed meridionally by the turbulent eddies. Here, therefore, the tracer measurements have been extrapolated by simulating the DIMES tracer release with a numerical model of the region, run at $1/20^{th}$ of a degree horizontal resolution. The model output is compared with hydrography and mooring observations (see Appendix B) and provides a link between the sub-sampled tracer distributions and the full tracer distribution.

Using the tracer sampled during the one-year tracer survey (called "US2"), together with the numerical model, we estimate that the tracer experienced a meridional isopycnal diffusivity of 710 ± 260 $\mathrm{m^2s^{-1}}$ over the first year after release. This value agrees with an independent estimate based on the dispersion of 72 acoustically-tracked isopycnal floats, deployed on the same isopycnal surface as the tracer (see LaCasce et al., 2014). The main objective of this paper is to explain how we obtained this estimate.

The isopycnal diffusivity estimated here is an isopycnal tracer diffusivity, not a lateral buoyancy diffusivity. That is, we are discussing the Redi diffusivity, not the Gent-McWilliams diffusivity using the jargon of non-eddy resolving climate models (see the discussion in the textbook by Griffies, 2004). The isopycnal diffusivity is also the diffusivity that mixes potential vorticity thereby driving the overturning ocean circulation (e.g. Plumb, 1986). The model suggests that the isopycnal tracer diffusivity increases from about 300 $\mathrm{m^2s^{-1}}$ in the upper ocean to 900 $\mathrm{m^2s^{-1}}$ at 2 km and decays rapidly below. The maximum in eddy diffusivity is near the steering level where the phase speed of the eddies equals the mean current speed. This is consistent with the suggestion that the zonal mean flows suppress mixing in the upper ocean, while the diffusivity is unsuppressed, and thereby enhanced, near the steering level (Smith and Marshall, 2009; Abernathey et al., 2010; Klocker et al., 2012b). The values of the diffusivity at the steering level from the present results are on the low side of those reported in the literature which span 1000–3000 $\mathrm{m^2s^{-1}}$ (Smith and Marshall, 2009; Klocker et al., 2012b; Abernathey et al., 2010). DIMES is the first study that relies on direct estimates of tracer spreading, while all previous studies were only indirectly constrained by data. Hence the DIMES estimates provide ground truth to derive better parameterizations of eddy mixing for climate models.

Our paper is organized as follows. The DIMES tracer release, sampling, measurements and uncertainty are discussed in Section 2. The numerical model and its comparison with observations are discussed in Section 3. Section 4 derives our best estimate of the eddy diffusivity based on DIMES data and model output. Section 5 describes the modeled estimates of the vertical dependence of diffusivity using a set of tracers released at different depths. We conclude in Section 6.

2 The DIMES tracer release

In early February 2009 (Cruise US1), 76 kg of a passive chemical tracer (trifluoromethyl sulphur pentaflouride, CF_3SF_5) were released from the Research Vessel *Roger Revelle* on the 27.9 kg m^{-3} neutral density surface (near 1500 m depth) upstream of the Drake Passage (58°S, 107°W) between the SAF and the PF (see Fig. 1a and Fig. 14). The tracer was released in a rough 'x' pattern in an area about 20 km across. The injection system was maintained within a few meters of the target isopycnal surface via a feedback control system, as described in Ledwell et al. (1998). The tracer distribution was sampled within two weeks of the release, and found to be confined to within 6 meters rms of the target density surface (Ledwell et al., 2011).

The tracer was intentionally released in fluid whose eastward motion was biased low, in order to facilitate initial sampling. The release location was guided by altimetry data indicating a stagnation point at depth, assuming the current to have an "equivalent barotropic" structure (Killworth and Hughes, 2002). Further evidence of a small velocity was obtained from a CTD survey conducted within 2 days of release in a 70-km box centered on the release site. The magnitude of the geostrophic velocity at the center of the tracer patch estimated from this survey, with surface geostrophic velocity from altimetry as reference, was less than 0.03 m/s. Low velocity of the tracer patch was at least partially confirmed by the observation that all of the stations at which tracer was found during the initial survey, 4 to 14 days after release, were within 10 km of the center of the initial patch.

In kinematic simulations based on the altimetry at the time of the experiment (not shown), with velocity at the tracer depth approximated as 0.38 times the surface geostrophic velocity from the altimeter, the center of mass of the tracer moved slightly to the west at first, and did not start moving east until a month after release. Thus, the actual tracer movement might be expected to have been delayed by about a month relative to the mean of an ensemble of numerical releases in other representations of the flow field.

The spread of the tracer was sampled during Cruise US2 (see Table 1), a year after the release, using a conventional CTD/Rosette system. Water samples were analyzed using a method similar to that described in Ho et al. (2008). The uncertainty (one standard deviation) of individual concentrations was no greater than 0.03×10^{-15} mol L^{-1}, or 5% of the concentration, whichever was greater. This uncertainty is small compared to the peak concentration measured during US2 of about 4×10^{-15} mol L^{-1}.

Fig. 1a shows the location of the initial tracer release on Cruise US1 (black dot) and the locations (circles) and normalized amounts of column-integrated tracer concentration measured (circle area) in the follow-up cruises: US2 (blue), UK2 (purple), UK2.5 (black) and US3 (red). The UK cruise tracks, which sample multiple transects, have been subdivided into individual transects UK2A, UK2B, UK2C, UK2.5A and UK2.5B. The areas of the circles in each cruise have been normalized by the maximum amount of tracer measured on that cruise, and the largest circles of each cruise have the same area (except US2 where due to high concentrations the largest circle has four times the area).

The column integral at each station was calculated by integrating over a profile obtained by interpolating linearly between the sample levels. Uncertainty of the column integrals is also less than 5%, which is very small compared with lateral variations, as assessed from the lateral autocorrelation of tracer integrals (not shown). The closest station spacing was 28 km, along the lines at 93°W and 96°W. The autocorrelation of column integrals of all station pairs with separation within 30 km (71 pairs) was only 0.4 ± 0.2. The autocorrelation decreases to 0 ± 0.2 for 121 pairs with separations between 90 and 120 km, which is less than the distance between major survey lines. Hence, accurate interpolation of the data to create a map is not possible even within the bounds of the survey. Furthermore, it is clear from the high levels of tracer found along the northern border of the survey (Fig. 1a) that although the survey may have delimited the tracer fairly well to the west and south, the patch was not delimited to the north and northeast.

The average of all the vertical profiles obtained during US2 was approximately Gaussian in shape with a standard deviation of 30 m, and with virtually all the tracer found within 100 m of the target density surface, as shown in Ledwell et al. (2011). Hence, one year after release, the vertical spread of the tracer was of the same order as the vertical resolution of most ocean circulation models, including the one used in the present study. Incidentally, variations among profiles of the vertical distribution were small enough that the estimate by Ledwell et al. (2011) of the diapycnal diffusivity, and its uncertainty, in the region between the injection location and the US2 survey area were accurate, despite the variability of column integral within the patch and the failure of the survey to delimit the patch.

Fig 2 shows column-integrated tracer concentrations divided by the total amount of tracer released (circles, units m^{-2}) for each of the cruises. Only a subset of Cruise US2 is shown: the latitudinal transect at 96°W denoted as 'US cruise 2A' and the latitudinal transect at 93°W denoted as 'US cruise 2B'. The x's with error bars shown in Fig. 2 represent simulated concentrations, which will be discussed in Section 3.2. The largest column integral measured during US2 was 3.46×10^{-9} mol m^{-2}, located at (94°W, 56.66°S), which, after normalizing by the 387.6 mols of injected tracer, is 8.92×10^{-12} m^{-2}. The maximum relative concentrations during UK2, UK2.5 and US3 were 1.05×10^{-12} m^{-2}, 9.55×10^{-13} m^{-2}, and 6.30×10^{-13} m^{-2} respectively. The maximum during US2 is an outlier twice as large as the next largest value during US2, which is itself 50% larger than the next 5–10 datapoints. Notice that the scale of the vertical axis in Fig. 2 decreases in downstream cruises because of dilution by dispersion and also because only the leading edge of the tracer patch is being sampled (UK2B, UK2C, UK2.5B) or the trailing edge of the tracer is being sampled (US3).

Cruise US2 is the only cruise where the tracer was sampled over a two dimensional grid, hence it is the only cruise from which the center of mass of the tracer can be estimated. The blue ‘x’ in Fig. 1b shows the center of mass of the DIMES tracer during US2, computed as $\overline{\mathbf{x}} = \sum_i(\mathbf{x}_i c_i)/\sum_i c_i$, and implies a slight southward displacement (about 0.75° latitude) and a mean zonal propagation speed of about 2.3 cm s^{-1} over the first year of dispersal. The trajectory of the center of mass followed very closely a constant streamline from the mean AVISO (CNES-CLS09 Version 1.1, Rio et al., 2011) dynamic topography.

3 The Drake Patch model

The simulated tracer data presented here are from a series of virtual tracer releases, which replicate the DIMES release, using a regional setup of the MITgcm (Marshall et al., 1997a,b), herein referred to as the “Drake Patch”. The model’s horizontal grid resolution is $1/20^{th}$ of a degree (a resolution of 3 km×6 km at the location of the tracer injection), spanning the Drake Passage from 160°W to 20°W in longitude and from 75°S to 35°S in latitude. The vertical mesh grid is divided into 100 layers of unequal thickness such that the top 70 layers, which span the top 1900 m, are all less than 35 m thick[1].

The European Centre for Medium-Range Weather Forecasts (ECMWF) Interim Reanaly-

[1] Layer spacing $\Delta z \leq 35$ m allows the vertical grid to resolve Gaussian tracer profiles with a root mean square spread as small as 70 m (Hill et al., 2012) and most importantly ensures that spurious numerical diffusion in the vertical is below 10^{-5} m^2s^{-1}, consistent with direct estimates of diapycnal diffusivity upstream of the Drake Passage from the DIMES tracer release (Ledwell et al., 2011).

sis (ERA-Interim, Simmons et al., 2006) 6-hour winds and buoyancy fluxes force the model's surface, and the Ocean Comprehensive Atlas (OCCA, Forget, 2009) provides monthly transports, heat and salt fluxes as well as sea ice area and thickness at the lateral boundaries. Initial model conditions are an interpolation of the $1^\circ \times 1^\circ$ resolution OCCA state on January 1, 2005, and the model cycles repeatedly over the years for which OCCA is defined (2004–2006). The simulations are intended to capture the statistics of the seasonal cycle and mesoscale of the Southern Ocean near the Drake Passage rather than predict the specific ocean state at the time of the DIMES tracer release. The model domain (excluding where restoring is applied to the OCCA state estimate) is shown in Figs. 3 and 4. A more detailed description of the model setup is given in Appendix B.

3.1 Comparison of the model with observations

We begin by comparing the Drake Passage transports, eddy kinetic energy and temperature-salinity hydrography with the Drake Patch simulation. The model vertically integrated zonal transport across the Drake Passage has a mean of 152 Sv and varies between 144 Sv and 162 Sv, with a standard deviation of 3 Sv, consistent with the transport entering from the open western boundary from OCCA (152 Sv, Forget, 2009). This transport is somewhat larger than past estimates (137$\pm$ 7 Sv, review by Meredith et al., 2011), but agrees with more recent ones (Firing et al., 2011, 154$\pm$ 38 Sv). The standard deviation is consistent with a recent eddying Southern Ocean state estimate (Mazloff, 2008), but much smaller than reported from observations, possibly because models underestimate the current temporal variability or because observational estimates are biased high due to poor temporal sampling especially at depth. We show below that tracers injected in the model move eastward at the same rate as the tracer released in DIMES, further confirming that the model eastward transport is consistent with observations.

The initial and boundary conditions in the Drake Patch are derived from the $1^\circ \times 1^\circ$ OCCA climatology which does not resolve eddies. Upon spinning up, boundary currents, baroclinic and barotropic instabilities and topographic steering quickly develop, in $\mathcal{O}(50)$ days, at and downstream of the Drake Passage (east of 75°W), as well as far upstream at the Udintsev and Eltanin fracture zones (between 145°W and 135°W). After $\mathcal{O}(100)$ days, a vigorous mesoscale eddy field is established in these regions. Weaker mesoscale eddies develop locally near the US2 region after $\mathcal{O}(300)$ days, and a significant amount of eddy kinetic energy is advected into the US2 region from the fracture zones to the west. An earlier model configuration, which had its western boundary at 115°W, and so lacked the upstream fracture zones, exhibited only about 60% of the eddy kinetic in a region near US2 (90°W – 100°W and 60°S–55°S) compared to the current configuration. Therefore, a significant amount of the eddy energy between 100°W and 80°W is advected into that region from the fracture zones at 140°W, despite the advective timescale for eddies to propagate 50 degrees downstream at 2.3 cm s^{-1} being about 4 years and the timescale of local baroclinic instability being less than a year (Tulloch et al., 2011). The simulation that includes Udintsev and Eltanin fracture zones also exhibits relatively more inter-annual variability of kinetic energy than the simulation without them and takes about twice as long to equilibrate at the surface (about 800 days versus 400 days to reach 90% of surface KE).

Figs. 3 and 4 compare mean and eddy current speeds in the Drake Patch model with AVISO altimetric observations. The model and the altimetric observations agree rather well, although the model's eddy kinetic energy is about 10% larger than AVISO near the US2 cruise track shown in Fig. 1a. The model's time-mean flow $(\overline{u}, \overline{v})$ is computed from a 3 year time-mean, while the AVISO speeds are based on a 19 year time-mean (1993-2011), so more eddy aliasing is present in the model time-means than in the AVISO time-means. This aliasing is likely responsible for some of the small scale features in the model average.

The model has a southward flowing boundary current off the coast of Chile that ejects northwest propagating anticyclonic eddies into the Pacific Ocean which are absent in the observations. These eddies are generated by the large freshwater fluxes along the Chilean coast[2] and they propagate away from the DIMES region. On the basis of our examination of water mass exchanges between the Chilean coastal region and the tracer sampling area, we do not expect freshwater fluxes to influence the tracer distribution during the first two years.

Fig. 5 compares the vertical structure of simulated root-mean-square current speed with observations from the First Dynamic Response and Kinematic Experiment (FDRAKE)

[2]An experiment with the atmospheric forcing shifted 20° west resulted in the generation of anticyclones 20 degrees west of the Chilean coast. These anticyclones appeared to be driven by freshwater forcing at the surface, as that region is one of the rainiest in the world, *e.g.,* Villa Puerto Edén receives almost 6 m of rain per year. They are likely sensitive to the ERA reanalysis product and its low resolution, which does not limit the heavy rain to the coastline.

moorings located in the Drake Passage during the late seventies (Pillsbury et al., 1979; Nowlin et al., 1982). The moorings were deployed for an average of about 320 days and corrected for blow-over (Nowlin et al., 1985). They are compared to a 3 year average in the model. The vertical decay of kinetic energy in the upper 3 km is very similar in model and observations, although the model is somewhat more energetic than the observations. The good match in the vertical decay of kinetic energy is important to support the analysis of lateral mixing at different depths presented below. The very energetic model vertical profile that lies to the right of all other profiles in Fig. 5 comes from the location of the northern-most mooring, which is close to the models strong boundary current, visible in Fig. 3b. This outlier profile is probably not very significant, because this current exhibits significant year to year variability in the model.

One possible reason for the energy level mismatch is due to missing ocean physics. While the model resolves mesoscale eddies, bottom boundary layer turbulence (Kantha and Clayson, 2000) and lee wave generation (Nikurashin and Ferrari, 2011; Nikurashin et al., 2013) are not well resolved, so the modeled eddies experience too little bottom dissipation. It may be possible to reduce the bias by a slight increase in quadratic bottom drag. In any case, our analysis focuses on mixing away from this boundary current.

Temperature, salinity and neutral density in the model upstream of the Drake Passage agree well with CTD data from the World Ocean Circulation Experiment (WOCE) and the Climate Variability (CLIVAR) programs. In Appendix B, Sections P18, P19C/S and A21 are compared with the model solution. The model receives large scale hydrographic information from OCCA at the western and northern boundaries, so the upstream sections in the model largely resemble OCCA and therefore observations. Within Drake Passage, the Polar Front appears to be shifted north by about one degree and is somewhat more intense. Section A21 appears to slice through a recirculation just north of 58°S in both observations and the model, a feature that is amplified in the model. While these differences may represent model bias, they are within the observed natural variability. For example, the Polar Front has been shown to meander between 57°S and 61°S (Dong et al., 2006): it was observed just south of 59°S during the DIMES experiment (Ledwell et al., 2012), close to 61°S in A21 (at 68∘W), and at 60°S in the Drake Patch model. The multi-year sea ice extent shown in Fig. 1a is also in reasonable agreement with observations.

3.2 Comparison with DIMES tracer measurements

We repeated 12 tracer injection experiments using the Drake Patch model. In each experiment the tracer was injected at the location of US1 in the DIMES field experiment. They were released 10 days apart from January through March of the 6$^{\mathrm{th}}$ year of model integration. The initial tracer distribution was a Gaussian blob in x, y and z ($\sigma_x = \sigma_y = 20$ km, $\sigma_z = 75$ m), with the vertical distribution centered on the 59$^{\mathrm{th}}$ model layer (1512 m depth), which is closest to the ρ_n =27.9 kg m^{-3} neutral density surface in the model in February.

Fig. 1a shows a snapshot of column integrated tracer concentration (in units of m^{-2}) after 365 days of integration for the tracer blob released on February 4 of the 6$^{\mathrm{th}}$ year of model integration. The tracer concentration shown is normalized by the maximum concentration in the domain, as was done for the tracer concentrations measured along each cruise and shown as circles, and all values between 0.5 and 1 have a uniform red tone. This is the same normalization used to display the tracer concentrations measured during the US2 cruise, one year after the DIMES release, and shown as blue circles. Tracer concentrations from later cruises (UK2A, UK2.5, US3) are also shown for reference.

The model tracer is still streaked into numerous filaments after one year (Fig. 1a). Much of the streakiness is eliminated in Fig. 1b which shows the distribution of the ensemble average of all 12 releases, 365 days after each of their respective starting times. The blue 'x' in Fig. 1b marks the center of mass of tracer collected during cruise US2 of the DIMES experiment, while the black 'x' ('+') marks the center of mass of the model ensemble average tracer sampled along the US2 cruise track (over the whole domain) at $t = 365$ days. The excess zonal distance travelled by the modeled tracer ensemble (1.2°) corresponds to an excess zonal propagation speed of the center of mass of 0.22 cm s^{-1} over the first year, compared to the DIMES tracer propagation speed of 2.3 cm s^{-1}. This difference is consistent with the fact that the DIMES tracer was purposefully released between the fronts in a region where the altimetric velocity was particularly weak–the tracer did not move east until a month after release, as discussed in Section 2.

Fig. 2 shows transect-by-transect comparisons of tracer concentrations observed in DIMES (gray circles) and the simulated ensemble average (black x's) for each of the cruises. Note that US2 has been split into its two main transects at 96°W (denoted US2A) and 93°W (US2B). The comparison indicates that, at least until UK2.5, the propagation and dispersion of the observed and simulated tracers are consistent. The ensemble tracer is generally less streaky than the observations because it is an average over 12 tracers. Some differences can be seen for the US3 transect. The model has more tracer north of 59°S than the observations and the observed tracer distribution is multimodal, while the modeled ensemble average concentration appears to be more Gaussian.

The time evolution of the mean and standard deviations of the modeled tracer concentration on the US2 cruise track stations are shown as black lines in Fig. 6a and 6c. The red x's mark the observed values, normalized by the total amount of tracer released. The mean concentration along a cruise track is defined as $\mu = N^{-1}\sum_i c_i$ and the standard deviation is defined as $s_N = \sqrt{(N-1)^{-1}\sum_i (c_i - \mu)^2}$, where N is the number of cruise track stations. The concentrations c_i are obtained by column-integrating the raw tracer concentrations, in mol L^{-1}, and then normalizing by the number of mols of CF_3SF_5 injected. The mean concentration reaches a maximum in the first 200 days and then decays as the tracer is advected toward the location of the US2 cruise track stations. The standard deviation, a measure of the tracer streakiness, instead peaks earlier at about 50 days. At the time of US2, the modeled streakiness has decayed to about $1/8^{\mathrm{th}}$ of its initial peak, as a result of lateral homogenization of the streaks. Both the modeled mean and standard deviations agree with observations, *i.e.,* the red error bar, defined as a 95% confidence interval using bootstrapping of the observed concentrations (Efron and Tibshirani, 1993; Zoubir and Boashash, 1998), overlaps the gray shading, which is the range spanned by the modeled ensemble members.

A summary comparison of the modeled and observed mean and standard deviations of tracer concentration along each of the cruise tracks, at the times of each cruise, is in Fig. 6b and 6d. As per Fig. 2, the mean and variance of concentrations on all of the cruises are consistent with observations, although the modeled concentrations are slightly larger for the US3 transect. The excess concentration in the model at the most northwest station of US3 indicate that the DIMES tracer might have taken a slightly more southerly path than the modeled tracer. UK2.5A and UK2.5B in Fig. 2 seem to be in agreement with this hypothesis, however UK2A and UK2B do not. Fig. 14f in Appendix B shows that the Polar Front in the model is displaced northwards compared to observations and probably explains these discrepancies.

4 Using passive tracers to estimate dispersion and isopycnal eddy diffusivity

In this section, we outline how we estimate the eddy diffusivity from the dispersion of a passive tracer released from a point source. We focus on cross-current diffusivity because it is the component that supports the MOC. The concentration of a tracer τ, within an isopycnal layer of thickness $z_\rho = \partial z / \partial \rho$, evolves according to the equation,

$$\partial_t \left(z_\rho \tau \right) + \nabla \cdot \left(\mathbf{u}_i z_\rho \tau \right) = 0 \tag{1}$$

where $\mathbf{u_i}$ is the along-isopycnal flow and the divergence is taken at constant density. Eq. (1) does not include a diapycnal flux, because Ledwell et al. (2011) reported very small diapycnal diffusivities of order of 10^{-5} m^{2}s^{-1} upstream of the Drake Passage at the tracer depth. The Drake Patch model has a similarly low diapycnal diffusivity $K^z < 10^{-5}$ m^{2}s^{-1} (see Appendix B). For such small diffusivities the diapycnal tracer flux is orders of magnitude smaller than the along-isopycnal one and can be ignored at leading order.

Taking an ensemble average over many tracer deployments, indicated with an overbar, we obtain an equation for the average amount of tracer within an isopycnal layer of thickness z_ρ,

$$\partial_t \overline{z_\rho \tau} + \nabla \cdot \overline{\mathbf{u}_i z_\rho \tau} = 0 \tag{2}$$

The thickness-averaged tracer flux can be decomposed into an advective and a diffusive component (Mazloff et al., 2013):

$$\partial_t \overline{z_\rho \tau} + \nabla \cdot \left(\overline{\mathbf{u}}^* \overline{z_\rho \tau}\right) = -\nabla \cdot \left(\overline{\hat{\mathbf{u}}\hat{\tau}}\bar{z}_\rho\right). \tag{3}$$

The advective component represents tracer transport of the thickness-averaged tracer by the thickness averaged velocity, $\overline{\mathbf{u}}^* = \overline{z_\rho \mathbf{u}_i}/\bar{z}_\rho$, which is the sum of the Eulerian and quasi-Stokes drift velocities (Plumb and Ferrari, 2005). The diffusive flux on the right hand side captures the along-isopycnal mixing by geostrophic eddies and it is given by the correlation of velocity and tracer fluctuations (hats are deviations from thickness averages.) If we assume that this flux is down the mean thickness-averaged tracer gradient (see Plumb and Ferrari, 2005), we obtain,

$$\partial_t \overline{z_\rho \tau} + \nabla \cdot \left(\overline{\mathbf{u}}^* \overline{z_\rho \tau}\right) = \nabla \cdot \left(\bar{z}_\rho \mathbf{K} \otimes \nabla \overline{\tau}^*\right), \tag{4}$$

where $\mathbf{K}$ is a 2×2 along-isopycnal eddy diffusivity tensor.

Figs. 3 and 4 suggest that both the mean and the eddy kinetic energies are uniform over the region of the tracer during the first year after injection (see Fig. 1). It is therefore sensible to assume that the components of the eddy diffusivity tensor do not vary much spatially. Furthermore the ACC mean flow is approximately zonal in the region and thus we can write $\overline{\mathbf{u}}^* = (u_0, 0)$. (The non-zonal mean flow problem is discussed in Appendix A, where we also comment on spatially variable diffusivities.) We also assume, without loss of generality, that the tracer center of mass is at $y = 0$. Under these assumptions, the meridional eddy diffusivity can be estimated multiplying Eq. (4) by y^2 and integrating over the density layers and lateral extent of the tracer patch. This gives the equation for the growth rate of the second meridional moment of the vertically integrated tracer concentration, as shown in Appendix A,

$$\partial_t \overline{\iiint y^2 \tau \ \mathrm{d}z\, dA} = 2\, K^{yy}\, \overline{\iiint \tau \ \mathrm{d}z\, dA}. \tag{5}$$

Thus if one measures the rate of change of the second moment of the vertically integrated tracer, across an ensemble of tracer releases, one can infer the diffusivity. This is the method used below.

Introducing the vertical integral of the tracer concentration $c = \int \tau \ \mathrm{d}z$ and the second moment of the tracer concentration $\sigma_y^2 \equiv \overline{\iint y^2 c \ \mathrm{d}A}$, Eq. (5) can be cast in the more familiar form first derived by Taylor (1921),

$$K^{yy} = \frac{1}{2} \frac{\partial_t \sigma_y^2}{\iint c \ \mathrm{d}A}. \tag{6}$$

The integral in the denominator will be equal to one in our calculations, because the tracer concentrations have been normalized with the total amount of tracer released.

For a meandering mean flow, one ought to use a coordinate system that tracks the mean streamlines of the ACC in order to separate the eddy diffusivity along and across the mean flow. In Appendix A, we show how to extend the expression for the eddy diffusivity to a curvilinear coordinate system (s, ψ), where s is the along-stream coordinate and ψ is the cross-stream coordinate. While the cross-streamline eddy diffusivity is mathematically well defined, it depends on curvature terms that are difficult to calculate accurately. Here, we chose to restrict the analysis upstream of the Drake Passage, west of 75°W, where the flow is mainly zonal and free of the strong meanders that exist downstream. The analysis in Appendix A confirms that the meridional and cross-streamline estimates of the eddy diffusivity are indistinguishable within error bars in the upstream region. In the interest of simplicity, we focus on the estimates of meridional diffusivity K^{yy}.

Another important consideration is whether the assumption of small longitudinal and latitudinal variations of K^{yy} in the ACC sector is supported by the tracer data. Strong support for this assumption comes from the analysis to follow, which shows that K^{yy} does asymptote to a constant value over the first year. K^{yy} would continue to vary, if the tracer kept sampling regions with different dispersion rates.

4.1 Estimates of dispersion from a deliberate tracer release

First we estimate the dispersion of the DIMES tracer after one year (US2) using available observations. Since only a fraction of the tracer was sampled during US2, any attempt of inferring the dispersion will be stymied by substantial uncertainty. We attempt to quantify this uncertainty by comparing a number of different approaches to estimating the rate of spreading experienced by the tracer after one year. Furthermore, any estimate of dispersion requires an average over many tracer release experiments as discussed in the previous section. But only one such release was done in the DIMES experiment. We will use the numerical model in the next section to determine how well one can infer dispersion from a single tracer release.

We consider three approaches to estimating the spreading of the tracer given by the centered second y-moment σ_y^2. The first method is a direct estimate of the second moment, that is $\sigma_y^2 = N^{-1} \sum_{i=1}^{N} {y'}_i^2 c_i$ where N is the number of stations occupied in US2, y'_i is the latitude of station i minus the latitude of the tracer center of mass, and c_i is the vertically integrated tracer concentration measured at that station. In the second method, the binned second moment, we first average all c_i in latitude bins, that is we average over longitude to obtain an estimate of the concentration as a function of latitude only. Then the centered second moment is computed from the concentration as a function of latitude. The third method does a least-squares Gaussian fit to the tracer concentration binned as a function of latitude and σ_y^2 is estimated as the variance of the Gaussian. In Appendix A we show that similar results are found using streamline coordinates, i.e. the spreading across streamlines is equal to the meridional spreading in the Drake Patch.

Estimates of σ_y^2 using each method are shown in Fig. 13. Each method has its strengths and weaknesses. The second moment method equally weights each datapoint assuming they are independent, and therefore tends to underestimate the dispersion when there is more sampling in the middle of the tracer distribution and when a significant fraction of the tracer is meridionally outside of the US2 sampling grid. The binned second moments alleviate the oversampling bias by first averaging tracer concentrations longitudinally and results in a slightly larger estimate. The bins are of equal width so bin averages are given equal weights. Binning introduces a new discretization error, but we found that binned estimates converged if more than 10 bins are used. The final method takes the binned values and minimizes the fit to a Gaussian distribution, to infer missing tracer. Rough interpolation estimates suggest that just less than 50% of the DIMES tracer was observed during US2, so fitting a Gaussian to the US2 data results in larger dispersion estimates.

Apart from the uncertainty due to the incomplete sampling of the tracer, additional uncertainty arises from converting the estimates of tracer dispersion into an estimate of eddy diffusivity. The eddy diffusivity is the asymptotic growth rate of σ_y^2. If the dispersion proceeded at the same rate throughout the whole year, then

$$K^{yy} = \frac{1}{2}\frac{d\sigma_y^2}{dt} = \frac{\sigma_y^2(1\text{year}) - \sigma_y^2(0)}{2\text{years}} \simeq \frac{\sigma_y^2(1\text{year})}{2\text{years}}. \tag{7}$$

However initial transients are expected during which the growth of the second moment is not linear in time. We return to this issue below, when we repeat the dispersion calculations with the numerical model. For the moment we treat Eq. (7) as an ansatz.

Table 2 reports estimates of K^{yy} based on Eq. (7) and the three methods outlined above for estimating $\sigma_y^2(1\text{year})$. Using the direct estimate of the second moment $K^{yy} = 407\ \text{m}^2\text{s}^{-1}$, while for the binned second moment $K^{yy} = 524\ \text{m}^2\text{s}^{-1}$ and the least-squares fit to a Gaussian gives $K^{yy} = 708\ \text{m}^2\text{s}^{-1}$. The second moment $K^{yy} = 407\ \text{m}^2\text{s}^{-1}$ is shown in Fig. 7 as a red 'x'. The errors bars around the 'x' in Fig. 7 correspond to the bracketed uncertainty ranges in Table 2, which are 95% confidence intervals computed by bootstrapping the sample data 10,000 times (Zoubir and Boashash, 1998).

Values of the eddy diffusivity K^{nn} in streamline coordinates are also reported in Table 2. These are obtained applying Eq. (7), but using $\sigma_\psi^2 = \langle \psi^2 c \rangle / \langle c \rangle$ instead of σ_y^2. They are substantially more uncertain, because of the additional complication of defining what are the proper mean streamlines. Analysis of the tracer spreading in the numerical model suggests that there is no advantage working in streamline coordinates in the region considered where the mean flow is very close to zonal. Results in streamline coordinates are compared with those in zonal coordinates in Appendix A.

The large range in estimates of eddy diffusivity confirms that incomplete sampling of the tracer contributes a large uncertainty. Furthermore, as will become more clear, all estimates ignore initial transients during which the growth of σ_y^2 is likely not linear in time. The model tracer release experiments will now be analyzed to gain insights on how to quantify both effects and obtain more robust estimates of the eddy diffusivity.

4.2 Estimates of dispersion and diffusivity from numerical tracers

The model is used to address three aspects of the tracer dispersion. First, we want to know whether the eddy diffusivity asymptotes to a constant over the first year. Second, we need to know whether we can use Eq. (7) to estimate the diffusivity. Third, we will consider the effect of under-sampling the tracer on estimates of the eddy diffusivity.

The blue line in Fig. 8a shows $\sigma_y^2(t)$ computed as the second moment of the ensemble tracer, i.e. the average over the 12 numerical injection experiments, using only tracer upstream of 75°W. East of 75°W, the tracer first gets squeezed into the Drake Passage and then veers north with the ACC resulting in rapid changes in the eddy statistics. For the first 500 days, out of the 1000 shown in the figure, the second moment increases approximately linearly in time. This confirms that the second moment of the tracer reaches a diffusive spreading within one year and it is sensible to represent this process with a constant eddy diffusivity.

The spreading of the ensemble mean tracer, the blue line in Fig. 8a, is not diffusive from day one. There is a small initial transient in the first 100 days when $\sigma_y^2(t)$ does not grow linearly with time. This transient reflects the relative dispersion that the tracer patch experiences before it reaches a size larger than the energy-containing eddies (LaCasce, 2008).

In order to assess whether this transient invalidates the use of Eq. (7), we least-squares fitted a line to $\sigma_y^2(t)$ between $t = 100$ days and $t = 500$ days (black line in Fig. 8a), and compared it to the red line which simply connects $\sigma_y^2(0)$ to $\sigma_y^2(1\text{year})$. The slope of the two lines are similar, 800 and 900 $\mathrm{m^2s^{-1}}$ respectively, suggesting that the ansatz of Eq. (7) is accurate to within 10%. Notice, however, that these estimates are based on an ensemble averaged tracer. In the DIMES experiment we have only one realization. In Fig. 8b we show, for each tracer release experiment, the half slopes estimated from linear least-squares fits between $t = 100$ days and $t = 500$ days, black 'x', versus the half slopes obtained from Eq. (7), red 'x'. Due the initial transient, estimates of K^{yy} based on Eq. (7) in the individual realizations vary from 718–966 m^2s^{-1}, whereas the dispersion rate from 100 to 500 days varies 727–861 m^2s^{-1}, which is a tighter bound on the diffusivity. Nevertheless, the differences between the two estimates are quite small and on average no larger than in the ensemble mean. We conclude that Eq. (7) can be used to estimate K^{yy} from data with perhaps a 20% uncertainty.

A more problematic issue in estimating the diffusivity is the extrapolation of the subsampled tracer on the US2 grid points to the full tracer distribution. Fig. 7 shows half the second moment of the US2 subsampled tracer divided by time (red line) and that for the full tracer upstream of the Drake Passage (black line); these are estimates of K^{yy} based on Eq. (7) applied at all times instead of only at one year. Second moments for the subsampled tracer are calculated using the first approach described in Section 4.1, that is, from all the individual column integrals, with no binning. The red line is 60% smaller than the black line implying that the US2 grid samples only a fraction of the tracer distribution. The ratio of the two curves is fairly constant between 250 and 450 days suggesting that estimates of K^{yy} based on sampling the tracers along the US2 grid after one year are biased 60% low.

The analysis presented so far suggests that Eq. (7) is appropriate to estimate K^{yy}, if the tracer is sampled adequately. Fig. 12 confirms that the estimate of K^{yy} is independent of the specific method used to estimate σ_y^2, when the calculation is applied to all of the tracer upstream of 75°W. Incomplete tracer sampling, however, as in the case of the DIMES experiment, is a serious limitation. Fig. 13 and Table 3 report estimates of K^{yy} computed using only data on the US2 cruise track. We repeated the same analysis followed for the

DIMES observations and used Eq. (7) with the three different approaches to estimate σ_y^2. The results are reported in Table 3. The model confirms that the second moment and the binned second moment methods strongly underestimate K^{yy}. The Gaussian fit method correctly extrapolates the missing tracer when applied to the ensemble averaged tracer on the US2 grid, but returns widely varying results when applied to a single tracer injection experiment. The inescapable conclusion is that none of the three approaches can be used to infer the spreading rate experienced by the tracer in DIMES, because the uncertainty associated with the missing tracer is too large.

Alternatively one can use the model estimate of K^{yy}, since the model has been tested against data. However, a comparison of data and model estimates based on tracer data on the US2 cruise track shows that the model estimates are biased high: see Tables 2 and 3 and Fig. 7. Although the error bars are large enough to make all estimates consistent (the model uncertainty is estimated as the range of values obtained from the 12 tracer release experiments, while the DIMES uncertainty is computed using bootstrapping), the high model bias is consistent with the model kinetic energy being somewhat too high as discussed in Section 3.1. It appears that the best way forward is to extrapolate the K^{yy} estimate from the DIMES data on the US2 cruise track using the model to infer the bias introduced because of the subsampling of the tracer. This is done in the next section.

4.3 Best estimate of the eddy diffusivity upstream of the Drake Passage at 1500 m

The tracer dispersion estimated from the DIMES data in Section 44.1 is likely an underestimate, because only half of the tracer was sampled and large values to the north suggest more dispersion northward. Since the model consistently overestimates the tracer dispersion compared to the DIMES observations, it cannot be used directly to estimate the DIMES diffusivity. We showed that by fitting a Gaussian meridionally to the subsampled tracer a Gaussian returned a diffusivity of $K^{yy} \approxeq \sigma_y^2(1\text{year})/2\text{years} \approx 708\ \text{m}^2\text{s}^{-1}$, but the uncertainty in this value is very large spanning the range 358-840 (see Table 2). Alternatively, the model can be used to infer how much of the tracer dispersion was missed by sampling only on the US2 cruise track.

Fig. 7 shows the extrapolation $\sigma_y^2|_{extrap}$ of the observed $\sigma_y^2|_{DIMES}$ from the US2 cruise multiplied by the ratio of the $\sigma_y^2|_{model\ full}$ estimated on the full domain west of 75°W (black line) and the $\sigma_y^2|_{model\ US2}$ estimated on the US2 cruise track only (red line),

$$\sigma_y^2|_{extrap} = \frac{\sigma_y^2|_{model\ full}}{\sigma_y^2|_{model\ US2}} \cdot \sigma_y^2|_{DIMES}. \tag{8}$$

The error in $\sigma_y^2|_{extrap}$ is estimated as

$$\text{Err } \sigma_y^2|_{extrap} = \sigma_y^2|_{extrap} \cdot \sqrt{\left(\frac{\text{Err } \sigma_y^2|_{DIMES}}{\sigma_y^2|_{DIMES}}\right)^2 + \left(\frac{\text{Err } \sigma_y^2|_{model\ US2}}{\sigma_y^2|_{model\ US2}}\right)^2}. \tag{9}$$

The error in the estimate of $\sigma_y^2|_{model\ US2}$ is calculated as the 95% confidence interval of the ensemble tracer dispersion on US2 computed using bootstrapping and is shown as grey shading in Fig. 7. The spread of $\sigma_y^2|_{model\ full}$ has not been included in the error estimate to avoid double counting. The observational error on $\sigma_y^2|_{DIMES}$ is estimated using bootstrapping and is shown as a red bar in Fig. 7.

The red ‘x’ in Fig. 7 marks the eddy diffusivity estimated using data along the US2 stations, while the blue ’x’ is the extrapolated value. The last two rows of Table 2 summarize the results. Using this extrapolation we estimate that the meridional eddy diffusivity in the DIMES experiment was 710±260 $\mathrm{m^2s^{-1}}$ at 1500m. This value agrees well with that estimated using a least-squares Gaussian fit, building confidence in our estimate.

5 Estimating the vertical structure of the eddy diffusivity

There is growing evidence that the isopycnal eddy diffusivity of passive tracers varies in the vertical and has subsurface maxima (Treguier, 1999; Smith and Marshall, 2009; Abernathey et al., 2010; Lu and Speer, 2010; Klocker et al., 2012b), unlike the horizontal buoyancy diffusivity which appears to be less variable in the vertical. It is therefore difficult to interpret the significance of the DIMES estimate and compare it to previous work without some information about the vertical variations from the 710 $\mathrm{m^2s^{-1}}$ value. We use the Drake Patch model to extrapolate the DIMES observations to the rest of the water column.

In order to assess the vertical variations of eddy diffusivity in the DIMES region, we ran an ensemble of tracers injected on February 4 of the 6$^{\mathrm{th}}$ year of model integration at 12 different depths between 500 m and 3500 m. The time evolution of σ_y^2 over time, estimated as the second moment of the tracer west of 75°W, is shown as blue lines for four selected depths in Fig. 9. After an initial transient of about 100 days, the shallowest tracer disperses approximately linearly with time until about $t = 500$ days. Afterwards the dispersion accelerates as most of the tracer has reached the Drake Passage (not shown). The red lines are the dispersion experienced by the tracer over the first year and its slope is given by Eq. (7); this is the estimate of the diffusivity used for the DIMES tracer in Section 4. The black line shows a linear least-squares fit to the dispersion between $t = 100$ days and $t = 500$ days, which attempts to remove the initial transient from the diffusivity estimate. For tracers released in the upper 1000m the slopes of the red and black curves are very different, because the effect of the initial transient is significant. It is actually difficult to select the time window over which the growth rate of σ_y^2 is linear and a diffusivity can be defined. The ACC flow gets stronger toward the surface and the tracer does not have much time to diffuse before reaching the Drake Passage: once the center of mass of the tracer reaches the Drake Passage, the flow first converges, resulting in a meridional squeezing of the tracer cloud, and then it veers north.

Fig. 10a shows the vertical profile of the diffusivity K^{yy} estimated by least-squares fitting lines between $t = 100$ days and $t = 500$ days (black line). The figure also shows the range of eddy diffusivity estimates from all 12 ensemble members released at 1500 m (thin horizontal black line) to emphasize that much uncertainty remains when the eddy diffusivity is estimated from a single release experiment. For comparison the best estimate of the eddy diffusivity from the DIMES tracer release is shown as a blue circle with its uncertainty. The model estimate is biased slightly too high, but well within the observational error bars.

Despite the uncertainty, Fig. 10a shows that the eddy diffusivity has a maximum between 1700 m and 2500m. Naively one may expect the eddy diffusivity to scale with the eddy kinetic energy, which is monotonically decreasing with depth as shown in Fig. 10b. However Bretherton (1966) and Green (1970) pointed out that mixing is strongly suppressed when eddies propagate at a speed different from the mean flow. Fig. 10b shows both the mean flow speed as a function of depth, averaged over the patch extending from 10W to 80W and 61S to 56S, and the eddy propagation speed, estimated with a radon transform of the sea surface height in the same region (see Smith and Marshall, 2009). The eddy propagation speed is much smaller than the mean flow speed in the upper kilometer, resulting in a suppression of the eddy diffusivity. Close to the steering level, where the mean flow equals the eddy propagation speed, there is no suppression and the eddy diffusivity is largest. Similar vertical profiles of eddy diffusivity have been reported in recent studies of ACC flows more or less constrained to observations (Smith and Marshall, 2009; Abernathey et al., 2010; Lu and Speer, 2010; Klocker et al., 2012b).

Based on the model results, we infer that the meridional eddy diffusivity in the DIMES region peaks at around 900 m^2s^{-1} between 1700 m and 2500 m, while it is smaller than 500 m^2s^{-1} in the upper kilometer. While this structure is consistent with recent studies, the absolute values of the diffusivity are less so. In particular Abernathey et al. (2010) and Klocker et al. (2012a) published larger estimates for the DIMES region. Abernathey et al. (2010) estimated the diffusivity advecting tracers with a state estimate of the Southern Ocean

Circulation and reported values around 500 m^2s^{-1} in the upper kilometer and values in excess of 2000 m^2s^{-1} at the steering level. Klocker et al. (2012a) estimated, using an idealized two-dimensional zonally re-entrant setup driven by surface altimetry, that the eddy diffusivity in the DIMES region peaked at 1000 m^2s^{-1} at 1.5 km depth, decreasing to 700 m^2s^{-1} at the surface. Most likely these differences stem from the different velocity fields use in the calculation and, in the case of Abernathey et al. (2010), from the use of a different method to compute the eddy diffusivity–they used Nakamura's definition of the eddy diffusivity. We believe that our estimate is more robust than these previous ones, because it is grounded in direct observations.

6 Discussion

This paper presents the first direct estimate of the isopycnal eddy diffusivity across the ACC just upstream of Drake Passage. The estimate was computed from the spreading of the DIMES tracer which was released in February, 2009. Using tracer sampling at one year after release (cruise US2) we estimated an isopycnal eddy diffusivity of 710 ± 260 m^2s^{-1} upstream of Drake Passage at 1500m. The estimate is based on the tracer spreading measured during US2 supplemented by a numerical model used to infer where the full tracer patch had spread after one year; US2 sampled only half of the tracer that was injected one year earlier.

In a companion paper LaCasce et al. (2014) find similar values of isopycnal eddy diffusivity from floats released during the DIMES field campaign and floats released in the same numerical model used in our study of tracer dispersion. This builds confidence that our estimate is accurate.

The numerical model further suggests that the isopycnal eddy diffusivity at 1500 m depth is close to its maximum in the water column. Diffusivities above 1000 m and below 3500 m appear to be smaller than 500 m^2s^{-1}. The maximum in eddy diffusivity coincides with the steering level where the eddy propagation speed of 2.2 cm s^{-1} matches the zonal mean flow (Fig. 10). This vertical profile is consistent with the notion that mixing is suppressed in the upper kilometer of the ocean where eddies propagate much slower than the strong ACC flow, while it is large at the steering level where there is no suppression (Bretherton, 1966; Green, 1970; Ferrari and Nikurashin, 2010). The mixing suppression at the surface and enhancement at depth is a robust feature of ocean mixing that has already been reported in idealized studies of channel flows (Treguier, 1999; Smith and Marshall, 2009), in studies informed by ACC observations (Abernathey et al., 2010; Lu and Speer, 2010; Klocker et al., 2012b) and in hydrographic sections (Naveira Garabato et al., 2011).

The present results have important implications for ocean models.The diffusivity estimated here is the Redi isopycnal diffusivity which homogenizes tracers and potential vorticity (Griffies, 2004). Our result is that the Redi diffusivity in a sector of the Southern Ocean varies in the vertical with a peak of approximately 900 m^2/s at 2 km. If these variations are not isolated to the region sampled in DIMES, they imply strongest ventilation at the interface between the upper and lower meridional overturning cells (Marshall and Speer, 2012) a region crucial for ocean carbon uptake. The implications for the horizontal buoyancy (Gent-McWilliams) diffusivity are more subtle. Smith and Marshall (2009) and

Abernathey et al. (2013) find that the buoyancy diffusivity is more vertically constant than the tracer diffusivity, and has a magnitude close to the surface value of the tracer diffusivity. If this holds true in general, our results imply that the buoyancy diffusivity is less than 500 m^2/s, a value smaller than presently used in ocean models used for climate studies. However we realize that our results apply only to a small sector of the Southern Ocean upstream of the Drake Passage and one cannot extrapolate the results to the global ocean. Rather our analysis provides a ground-truth for developing parameterizations, which can then be used to extrapolate our results to other regions. A new parameterization of eddy mixing based on these results is currently being developed (Bates et al., 2013).

Acknowledgments. Ferrari and Tulloch wrote the manuscript with input from the other co-authors. Ledwell, Messiah, Speer and Watson led the tracer field measurements. Ferrari, Jahn, Klocker, LaCasce, Marshall and Tulloch led the numerical simulation work. We wish also to thank all the scientists and ship crews of DIMES for their many contributions to a very successful experiment. NSF support through awards OCE-1233832, OCE-1232962 and OCE-1048926 is gratefully acknowledged. Computing resources on Pleiades and Yellowstone proved essential to perform the numerical simulations that are used to interpret the data.

Appendix A: Computation of tracer dispersion

The goal of this paper is to quantify the mixing by geostrophic eddies along isopycnal surfaces and across mean currents. It is thus necessary to use a coordinate system that follows isopycnal surfaces and mean streamlines. We discuss the transformation to isopycnal coordinates first, and then we tackle the rotation into a streamline coordinate system.

A.1 Tracer moments in isopycnal coordinates

The equation for the temporal growth rate of the vertically integrated tracer,

$$\sigma_y^2 = \iiint y^2\, \overline{z_\rho \tau}\ \mathrm{d}\rho \mathrm{d}A = \overline{\iiint y^2 \tau\ \mathrm{d}z \mathrm{d}A}, \tag{10}$$

is obtained multiplying the thickness averaged tracer equation (4) by y^2 and integrating over density and in the horizontal beyond where there is any tracer. The final result is given in Eq. (6) in the main text. Here are provide few more steps to help follow the full derivation,

$$\begin{aligned}
\partial_t \overline{\iiint y^2 \tau\ \mathrm{d}z \mathrm{d}A} &= -2K \iiint y \partial_y \overline{\tau}^* \mathrm{d}\bar{z} \mathrm{d}A && (11)\\
&= 2K \iiint \overline{\tau}^* \mathrm{d}\bar{z} \mathrm{d}A && (12)\\
&= 2K \iiint \overline{z_\rho \tau}\ \mathrm{d}\rho \mathrm{d}A && (13)\\
&= 2K \overline{\iiint \tau\ \mathrm{d}z dA}. && (14)
\end{aligned}$$

A.2 Tracer moments in streamline coordinates

Isopycnal mixing by geostrophic eddies is generally strongly anisotropic, being much larger along mean currents than across. It is therefore necessary to rotate coordinates along and across mean streamlines to properly estimate mixing in the two directions. We could not find a description of how to compute eddy diffusivities in a streamline coordinate system and so we decided to include in this appendix the details involved in the calculations. The second section of the appendix then compares estimates of the dispersion in streamline and longitude-latitude coordinates for the DIMES region.

The mean coordinate system is defined through a 2D streamline coordinate system (s,ψ) where s is the along-stream coordinate (with units of length) and ψ is the cross-stream coordinate which increases normal ($\hat{\mathbf{n}}$) to the stream, *i.e.,*

$$\hat{\mathbf{s}} = \frac{\mathbf{k} \times \nabla\psi}{|\nabla\psi|}, \qquad \hat{\mathbf{n}} = \frac{\nabla\psi}{|\nabla\psi|}.$$

as shown in the Fig. 11 below. The streamline may represent the barotropic streamfunction but also the streamfuction at some level, if the flow is equivalent barotropic as appears to be the case in the ACC (Killworth and Hughes, 2002).

The first step is to write in streamline coordinates the conservation equation for the vertically and ensemble averaged tracer $\overline{c}$ advected by a two-dimensional streamfunction ψ,

$$\partial_t \overline{c} + J(\psi, \overline{c}) = -\nabla \cdot \mathbf{F}, \tag{15}$$

where J is a two-dimensional Jacobian and $\mathbf{F}$ represents the eddy flux of tracer. The flux term in streamline coordinates takes the form,

$$\nabla \cdot \mathbf{F} = |\nabla\psi| \left[\frac{\partial}{\partial s} \left(\frac{\mathbf{F} \cdot \hat{\mathbf{s}}}{|\nabla\psi|} \right) + \frac{\partial}{\partial \psi} \left(\mathbf{F} \cdot \hat{\mathbf{n}} \right) \right]. \tag{16}$$

In order to find an expression for the cross-streamline flux, we average the tracer equation along a streamline. First consider the average of a generic function $F(x, y)$ over a region encircled by a stream function ψ,

$$I(\psi) = \int_{R_\psi} F(x,y)dA.$$

Following Young (1981, pg. 84, Eq. 9.13), we take the derivative of $I(\psi)$ with respect to ψ, which is the average of $F(x,y)$ along the streamline,

$$\begin{aligned}
\frac{dI(\psi)}{d\psi} &= \lim_{\Delta\psi\to 0} \frac{I(\psi+\Delta\psi) - I(\psi)}{\Delta\psi} \\
&= \lim_{\Delta\psi\to 0} \frac{1}{\Delta\psi} \left[\int_{R_\psi+\Delta\psi} F(x,y)ds\frac{d\psi}{|\nabla\psi|} - \int_{R_\psi} F(x,y)ds\frac{d\psi}{|\nabla\psi|} \right] \\
&= \oint_{\partial R_\psi} F\frac{ds}{|\nabla\psi|}.
\end{aligned}$$

The eddy flux is now assumed to be related to the mean tracer gradient through a diffusivity tensor $\mathbf{K}$,

$$\mathbf{F} = -\mathbf{K} \otimes \nabla\overline{\mathbf{c}}. \tag{17}$$

Integrating the tracer equation along a streamline then gives

$$\partial_t \oint_{\partial R_\psi} \overline{c}\frac{ds}{|\nabla\psi|} + \oint_{\partial R_\psi} \nabla\overline{c}\cdot d\mathbf{s} = \oint_{\partial R_\psi} \left[\frac{\partial}{\partial s}\left(\frac{\mathbf{K}\otimes\nabla\overline{\mathbf{c}}\cdot\hat{\mathbf{s}}}{|\nabla\psi|} \right) + \frac{\partial}{\partial\psi}\left(\mathbf{K}\otimes\nabla\overline{\mathbf{c}}\cdot\hat{\mathbf{n}}\right). \right] ds$$

Assuming that the streamline average extends over the whole region where there is some tracer, one has,

$$\partial_t \oint_{\partial R_\psi} \overline{c}\frac{ds}{|\nabla\psi|} = \oint_{\partial R_\psi} \frac{\partial}{\partial\psi}\left(\mathbf{K}\otimes\nabla\overline{\mathbf{c}}\cdot\hat{\mathbf{n}}\right) ds.$$

The diffusivity tensor, which can be decomposed into anti-symmetric and symmetric components as $\mathbf{K} = \mathbf{K^{asym}} + \mathbf{K^{sym}}$,

$$\mathbf{K^{asym}} = \begin{pmatrix} 0 & -K^a \\ K^a & 0 \end{pmatrix}, \qquad \mathbf{K^{sym}} = \begin{pmatrix} K^{ss} & K^{sn} \\ K^{ns} & K^{ss} \end{pmatrix}. \tag{18}$$

Expanding $\mathbf{K}$ into its tensor components gives

$$\partial_t \oint \overline{c} \frac{ds}{|\nabla \psi|} = \oint \frac{\partial}{\partial \psi} \left((K^a + K^{ns}) \frac{\partial \overline{c}}{\partial s} + K^{nn} |\nabla \psi| \frac{\partial \overline{c}}{\partial \psi} \right) ds. \tag{19}$$

Under the assumption that the diffusivity tensor is independent of the along stream coordinate, *i.e.,* $\mathbf{K} = \mathbf{K}(\psi)$, the $\partial_s \overline{c}$ term in Eq. (19) integrates to zero so the cross-stream diffusivity K^{nn} is the only component that evolves the stream-averaged tracer.

Further integrating Eq. (19) over the cross-stream coordinate gives the equation for the tracer averaged over the full domain,

$$\partial_t < \overline{c} > = \partial_t \iint \overline{c} \frac{ds}{|\nabla \psi|} d\psi = \iint \frac{\partial}{\partial \psi} \left(K^{nn} \nabla \overline{c} \cdot \hat{\mathbf{n}} \right) d\psi ds = 0.$$

Integrating the first moment with respect to ψ gives,

$$\begin{aligned} \partial_t < \psi \overline{c} > &= \iint \psi \frac{\partial}{\partial \psi} \left(K^{nn} \nabla \overline{c} \cdot \hat{\mathbf{n}} \right) d\psi ds \\ &= \iint \left(\frac{\partial K^{nn}}{\partial \psi} |\nabla \psi|^2 + \frac{1}{2} K^{nn} \frac{\partial}{\partial \psi} |\nabla \psi|^2 \right) \overline{c} \; dA, \end{aligned} \tag{20}$$

which implies a shift of the center of mass towards larger ψ, if either the diffusivity or the mean flow increase with ψ ($\partial_\psi K^{nn} > 0$ or the streamlines become more packed).

Integrating the second moment with respect to ψ gives

$$\begin{aligned} \partial_t < \psi^2 \overline{c} > &= \iint \psi^2 \frac{\partial}{\partial \psi} \left(K^{nn} \nabla \overline{c} \cdot \hat{\mathbf{n}} \right) d\psi ds \\ &= 2 \iint \left(\frac{\partial K^{nn}}{\partial \psi} |\nabla \psi|^2 \psi + K^{nn} |\nabla \psi|^2 + \frac{1}{2} K^{nn} \psi \frac{\partial}{\partial \psi} |\nabla \psi|^2 \right) \overline{c} \; dA, \end{aligned} \tag{21}$$

so dispersion in stream coordinates depends on the cross gradient of the diffusivity and mean flow speed.

When the cross-gradient diffusivity K^{nn} is approximately uniform ($\partial_\psi K^{nn} \to 0$) then the cross-stream diffusivity is approximately

$$K^{nn} = \frac{1}{2} \frac{\partial_t < \psi^2 \overline{c} >}{< \left(|\nabla \psi|^2 + \frac{1}{2} \psi \frac{\partial}{\partial \psi} |\nabla \psi|^2 \right) \overline{c} >}. \tag{22}$$

If the curvature of the streamlines is small, $\psi\, \partial_\psi (|\nabla \psi|^2) \ll |\nabla \psi|^2$, then the expression for K^{nn} reduces to

$$K^{nn} \simeq \frac{1}{2} \frac{\partial_t < \psi^2 \overline{c} >}{< |\nabla \psi|^2 \overline{c} >}. \tag{23}$$

The $|\nabla \psi|^2$ factor in the denominator represents that the conversion between dispersion in ψ coordinates and length coordinates.

Finally note that if the center of mass of the tracer in streamline coordinates is not at $\psi = 0$, i.e. $< \psi \overline{c} > \neq 0$, then the dispersion must be calculated as the growth rate of the centered second moment. In the following calculations, we will set $\psi = 0$ for the streamline along which the tracer was released.

A.3 Estimates of tracer dispersion across streamlines in the Drake Patch

We introduced three different estimators of σ_y^2 in latitude coordinates in Section 4.1. We now compare those estimates to equivalent ones in streamline coordinates to test whether the assumption that the flow in the DIMES region is zonal is sufficiently accurate for our calculations. We choose the time-mean surface geostrophic streamfunction $\psi = g\eta/f$, where g is the gravitational constant, η is sea surface height and f is the local Coriolis frequency, to define our streamlines. Fig. 12 shows estimates of K^{yy} (top) and K^{nn} (bottom) versus time using the three methods described in Section 4.1: a second moment which assumes all data points are independent, a binned second moment averaged along the stream (zonally) within cross-stream (meridional) bins, and a least-squares fit to a Gaussian distribution using the binned data (left to right). To define the streamlines, the model's sea surface height was averaged from year 5 to 10, then coarse-grain averaged using a Shapiro (1970) filter to remove eddy aliasing. In order to smooth the diffusivity in time, we plot the time-integrated rate of dispersion $K^{yy} = \sigma_y^2/2t$ rather than the instantaneous rate of dispersion defined in Eq. (6). As the tracer enters the Drake Passage, the streamlines bend and turn northward. This turning northward artificially increases K^{yy} and the bending would make the curvature term in the denominator of Eq. (22) for K^{nn} significant. Also, narrowing of the stream in and downstream of the Drake Passage likely invalidates the assumption that $\partial_\psi K^{nn} \to 0$. To alleviate all of these issues we have restricted the tracer dispersion calculations shown in Fig. 12 to tracer that is west of 75°W, which encompasses nearly all of the tracer shown in Fig. 1 at t =1 year.

In the left panels of Fig. 12, the dispersion is integrated exactly as defined in the equations above. In the middle panels, meridional and cross-stream bins of equal width (25 bins, 1/2 of a degree apart in latitude from 65°S to 53°S), and an equivalent bin width in ψ of approximately 4×10^3 m^{2}s^{-1}) are defined to bin the tracer before summing across the stream. This calculation is essentially identical to the method on the left, but with less cross-stream resolution. In the right panels, the tracer is first binned as in the middle panels and then fitted to a meridional or cross-stream Gaussian profile via least-squares gradient descent, analogously to the method used in Ledwell et al. (1998). Fig. 12 shows that the three methods shown agree with each other when the full (upstream) tracer is taken into account, and that the latitudinal and cross-stream diffusivities are both approximately $K = 800 - 1000 \text{ m}^2\text{s}^{-1}$ in the model at $t = 1$ year. When the full tracer is known, the estimates on the right agree with the estimates on the left in the ensemble mean (thick black line), but there is more uncertainty in the ensemble members (thin gray lines). The middle and left plots also decrease at later times as more of the tracer approaches the Drake Passage where the stream is slightly narrower, while this effect seems to be absent in the least-squares fits on the right. The cross-stream diffusivities are a bit larger than the latitudinal diffusivities (Table 3), but the differences are not significant compared with the uncertainties.

A.4 Estimates of tracer dispersion across streamlines in DIMES

Fig. 13 shows estimates of eddy diffusivity using the same three methods described in Section 4.1, but using streamlines coordinates. The second moment of the tracer in streamline coordinates is estimated as $\sigma_\psi^2 = \langle \psi^2 c \rangle / \langle |\nabla \psi|^2 c \rangle$ and data are averaged in streamline bins instead of latitude bins for the bin averages. We did not include the additional curvature terms, because they simply add noise to the estimates. The mean dynamic topography from AVISO (CNES-CLS09 Version 1.1, Rio et al., 2011) is used to define the streamfunction coordinate system. The estimates using streamfunction coordinates are slightly smaller for all methods, but the uncertainty range is larger. Estimates using streamfunction coordinates are again similar to those obtained using latitude coordinates but somewhat smaller because the streamlines are not perfectly zonal and the tracer center of mass drifts south over the first year by about 0.5–0.75° (Fig. 13 and Table 3).

Appendix B: Model setup and comparison with hydrography

The Drake Patch model is a regional configuration of the MITgcm, on a $1/20^{th}$ of a degree resolution latitude-longitude grid. Horizontal vorticity is advected with a fourth-order accurate spatial discretization using an enstrophy conserving (Arakawa and Lamb, 1977) and vector invariant formulation. Horizontal viscosity is biharmonic, with an amplitude that scales according to local grid spacing and stresses (Fox-Kemper and Menemenlis, 2008). Vertical viscosity is Laplacian and a quadratic bottom drag is imposed in the lowest layer. Momentum, temperature and salinity are forced at the surface by re-analysis from the European Centre for Medium Range Weather Forecasts (ECMWF ERA-Interim) on a 6-hourly timescale and at approximately 0.7 degree resolution (Dee et al., 2011). The initial hydrography is taken from an average of OCCA's December 2004 and January 2005 fields (Forget, 2010). There is dynamic sea ice, and the freezing temperature is set to $T = 273.2501 - 0.0575 \cdot S$. Advection of temperature, salinity and passive tracers is by a spatially seventh-order accurate, monotonicity preserving scheme (Daru and Tenaud, 2004). The K-profile parameterization scheme of Large et al. (1994)

is used to parameterize vertical mixing due to boundary layer shear and convective instability. Table 4 summarizes the numerical parameters. The bathymetry was downloaded from `ftp://topex.ucsd.edu/pub/srtm30\_plus/topo1\_topo2/topo1.grd` and is David Sandwell's SRTM30_PLUS V7 averaged to $1/20^{\text{th}}$ of a degree from one minute (Smith and Sandwell, 2004). The model includes the MITgcms sea-ice thermodynamic model with standard settings (Losch et al., 2010). Bulk formulae are used to compute the atmospheric heat and fresh water flux from the changing sea surface temperature (Large and Yeager, 2004).

Lateral boundary conditions (U, V, S, T, and sea ice) on a monthly time scale and one degree resolution from OCCA are interpolated onto the model's resolution. A relaxation boundary condition absorbs outgoing flow over a one degree sponge layer (see Section 6.3.2 of MITgcm Group, 2011, for details of the MITgcm relaxing boundary condition scheme). The model cycles repeatedly over the three years for which OCCA is defined (2004-2006). Tracers are injected once the model has cycled 1.66 times through the OCCA three year period. The OCCA boundary conditions are interpolated in time to avoid any shocks in the dynamics and tracer evolution.

B.1 Comparison of Drake Patch model against hydrography

Fig. 14 compares the model's hydrography (right plots) with CTD data stored at the CLIVAR & Carbon Hydrographic Data Office (left plots) from sections P18 (top), P19 (middle), and A21 (bottom), which are denoted with gray dashed lines in Fig. 3. The westernmost section, P18 at 103°W, is in a relatively quiescent region of the ACC, near the initial DIMES tracer injection point. The SAF is visible at (103°W, 55°S) and PF at (103°W, 60°S) in both the model and in P18. North of 60°S there appears to be a deeper mixed layer, or mode water, in the model compared to observations. Deeper model mixed layers are expected because the model does not have a submesoscale parameterization for mixed layer restratification (Fox-Kemper and Ferrari, 2008). At P19 (88°W), the fronts appear to be sharper south of 60°S in the model than in observations possibly due to the different sampling resolution of model versus ships or to the lacking representation of bottom dissipation processes in the model. There is also more mode water present at P19 in the model than in observations. Within the Drake Passage, at Section A21, the SAF appears similar between the model and observations, but the PF is stronger in the model and displaced northwards by about half a degree. There also appears to be a bowl of low density water in the model between 60°S and 58°S, which does not appear in the observations below 1 km. The bowl of low density water in the model likely results from the path of the ACC in the model along A21, visible in Fig. 3b. The transect appears to run almost parallel to the jet at 58.5°S.

B.2 Vertical diffusivity in the model

Ledwell et al. (2011) showed that diapycnal diffusivity upstream of the Drake Passage is approximately 1.3×10^{-5} m^{2}s^{-1} at 1500 m depth. However many eddying z-coordinate models contain a horizontal bias as isopycnal surfaces become steeply inclined, which can lead to numerically generated diapycnal mixing of the order of 10^{-4} m^{2}s^{-1} (Griffies et al., 2000). Hill et al. (2012) show that this spurious diapycnal mixing can be limited to $K^{zz} < 10^{-5}$ m^{2}s^{-1}

when the vertical tracer variations are well-resolved and a second order moment (SOM) advection scheme (Prather, 1986) is employed. Specifically, for a tracer with a Gaussian concentration and a vertical standard deviation of 50 m and layer thicknesses of 10 m, they obtain a diapycnal diffusivity of about 0.5×10^{-5} $\mathrm{m^2s^{-1}}$ using the SOM scheme with a flux limiter (their simulation A2). However when the Gaussian profile is not well resolved, *i.e.,* layer thicknesses of 100 m, the flux limited scheme produces 8 times more diapycnal diffusivity. Without a flux limiter (simulation A1) the diffusivity stays under 10^{-5} $\mathrm{m^2s^{-1}}$.

Fig. 15 shows the evolution of tracer variance in density space in the Drake Patch model for a single tracer released with a Gaussian initial profile with half-width $\sigma_z = 75$ m, using the SOM advection scheme without flux limiter and a 7th-order, one-step, monotonicity preserving method (Daru and Tenaud, 2004). All layers shallower than 2 km in the Drake Patch are thinner than 35 m, so this tracer, centered at 1500 m is well resolved in the vertical. Converting from variance in density coordinates to height coordinates using the average neutral density gradient at 1500 m as $d\rho_n/dz \approx -3.8 \times 10^{-4}$kg $\mathrm{m^{-4}}$ yields $K^{zz} < 10^{-5}$ $\mathrm{m^2s^{-1}}$ for both advection schemes.

References

Abernathey, R. P., D. Ferreira, and A. Klocker, 2013: Diagnostics of eddy mixing in a circumpolar channel. *Ocean Modell.*, Submitted.

Abernathey, R. P., J. Marshall, and D. Ferreira, 2011: The dependence of Southern Ocean meridional overturning on wind stress. *Journal of Physical Oceanography*, **41**, 2261–2278, doi:10.1175/JPO-D-11-023.1.

Abernathey, R. P., J. Marshall, and M. Mazloff, 2010: Enhancement of mesoscale eddy stirring at steering levels in the Southern Ocean. *Journal of Physical Oceanography*, **40**, 170–184, doi:10.1175/2009JPO4201.1.

Arakawa, A. and V. Lamb, 1977: Computational design of the basic dynamical processes of the UCLA general circulation model. *Methods in Computational Physics*, Academic Press, volume 17, 174–267.

Bates, M., R. Tulloch, J. Marshall, and R. Ferrari, 2013: Rationalizing the spatial distribution of mesoscale eddy diffusivity in terms of mixing length theory. *JPO*, **43**, under review.

Bretherton, F. P., 1966: Critical layer instability in baroclinic flows. *Quart. J. Roy. Meteor. Soc.*, **92**, 325–334.

Daru, V. and C. Tenaud, 2004: High order one-step monotonicity-preserving schemes for unsteady compressible flow calculations. *J. Comput. Phys.*, **193**, 563–594.

Dee, D. P., S. M. Uppala, A. J. Simmons, P. Berrisford, P. Poli, S. Kobayashi, U. Andrae, M. A. Balmaseda, G. Balsamo, P. Bauer, P. Bechtold, A. C. M. Beljaars, L. van de Berg, J. Bidlot, N. Bormann, C. Delsol, R. Dragani, M. Fuentes, A. J. Geer, L. Haimberger, S. B. Healy, H. Hersbach, E. V. Hlm, L. Isaksen, P. Kllberg, M. Khler, M. Matricardi, A. P. McNally, B. M. Monge-Sanz, J.-J. Morcrette, B.-K. Park, C. Peubey, P. de Rosnay, C. Tavolato, J.-N. Thpaut, and F. Vitart, 2011: The ERA-Interim reanalysis: configuration and performance of the data assimilation system. *Quart. J. Roy. Meteor. Soc.*, **137**, 553–597, doi:10.1002/qj.828.

Dong, S., J. Sprintall, and S. T. Gille, 2006: Location of the antarctic polar front from amsr-e satellite sea surface temperature measurements. *Journal of Physical Oceanography*, **36**, 2075–2089.

Efron, B. and R. Tibshirani, 1993: *An Introduction to the Bootstrap*. Chapman and Hall, New York, USA, 1 edition, 456 pp.

Ferrari, R. and M. Nikurashin, 2010: Suppression of eddy diffusivity across jets in the Southern Ocean. *Journal of Physical Oceanography*, **40**, 1501–1519, doi:10.1175/2010JPO4278.1.

Firing, Y. L., T. K. Chereskin, and M. R. Mazloff, 2011: Vertical structure and transport of the Antarctic Circumpolar Current in Drake Passage. *J. Geophys. Res.*, **116**, C08015, doi:10.1029/2011JC006999.

Forget, G., 2009: Mapping ocean observations in a dynamical framework: a 2004-2006 ocean atlas. *Journal of Physical Oceanography*, **39**, doi:DOI: 10.1175/2009JPO4043.1.

— 2010: Mapping ocean observations in a dynamical framework: A 2004–2006 ocean atlas. *Journal of Physical Oceanography*, **40**, 1201–1221.

Fox-Kemper, B. and R. Ferrari, 2008: Parameterization of mixed layer eddies. part ii: Prognosis and impact. *Journal of Physical Oceanography*, **38**, 1166–1179.

Fox-Kemper, B. and D. Menemenlis, 2008: Can large eddy simulation techniques improve mesoscale rich ocean models? *Ocean Modeling in an Eddying Regime*, M. Hecht and H. Hasumi, eds., American Geophysical Union, volume 177, 319–338.

Green, J. S. A., 1970: Transfer properties of the large-scale eddies and the general circulation of the atmosphere. *Quart. J. Roy. Meteor. Soc.*, **96**, 157–185.

Griffies, S. M., 2004: *Fundamentals of Ocean Climate Models*. Princeton University Press, Princeton, 1st edition.

Griffies, S. M., R. C. Pacanowski, and R. W. Hallberg, 2000: Spurious dyapycnal mixing associated with advection in a z-coordinate ocean model. *Mon. Wea. Rev.*, **128**, 538–564.

Hill, C., D. Ferreira, J.-M. Campin, J. Marshall, R. Abernathey, and N. Barrier, 2012: Controlling spurious diapycnal mixing in eddy resolving height-coordinate ocean models-insights from virtual deliberate tracer release experiments. *Ocean Modell.*, **45–46**, 14–26, doi:10.1016/j.ocemod.2011.12.001.

Ho, D. T., J. R. Ledwell, and W. M. Smithie Jr., 2008: Use of SF_5CF_3 for ocean tracer release experiments. *Geophysical Research Letters*, **35**, L04602, doi:10.1029/2007GL032799.

Johnson, G. C. and H. L. Bryden, 1989: On the size of the Antarctic Circumpolar Current. *Deep-Sea Res.*, **36**, 39–53.

Kantha, L. H. and C. A. Clayson, 2000: *Small Scale Processes in Geophysical Fluid Flows*. Academic Press, San Francisco, USA, 1 edition, 750 pp.

Killworth, P. D. and C. W. Hughes, 2002: Boundary conditions on quasi-stokes velocities in parameterizations. *J. Mar. Res.*, **60**, 19–45.

Klocker, A., R. Ferrari, and J. H. LaCasce, 2012a: Estimating suppression of eddy mixing by mean flows. *Journal of Physical Oceanography*, **42**, 1566–1576.

Klocker, A., R. Ferrari, J. H. LaCasce, and S. Merrifield, 2012b: Reconciling float-based and tracer-based estimates of lateral diffusivities. *J. Marine Res.*, **70**, 569–602.

LaCasce, J. H., 2008: Statistics from lagrangian observations. *Prog. Oceanography*, **77**, 1–29.

LaCasce, J. H., R. Ferrari, R. Tulloch, J. Marshall, D. Balwada, and K. Speer, 2014: Float-derived isopycnal diffusivities in the DIMES experiment. *JPO*, **44**, 764–780.

Large, W., J. McWilliams, and S. Doney, 1994: Oceanic vertical mixing: A review and a model with nonlocal boundary layer parameterization. *Rev. Geophys.*, **32**, 363–403.

Large, W. and S. Yeager, 2004: Diurnal to decadal global forcing for ocean and sea-ice models: The data sets and flux climatologies. Technical report, NCAR, technical Report TN-460+STR.

Ledwell, J. R., L. C. St. Laurent, J. B. Girton, and J. M. Toole, 2011: Diapycnal mixing in the antarctic circumpolar current. *Journal of Physical Oceanography*, **41**, 241–246, doi:10.1175/2010JPO4557.1.

— 2012: Diapycnal mixing in the antarctic circumpolar current. *Journal of Physical Oceanography*, **42**, 2143–2152, doi:10.1175/JPO-D-12-027.1.

Ledwell, J. R., A. J. Watson, and S. S. Law, 1998: Mixing of a tracer in the pycnocline. *J. Geophys. Res.*, **103**, 21499–21529.

Losch, M., D. Menemelis, J. M. Campin, P. Heimbach, and C. Hill, 2010: On the formulation of sea-ice models. part 1: Effects of different solver implementations and parameterizations. *Oceanogr. Meteor.*, **33**, 129–144.

Lu, J. and K. Speer, 2010: Topography, jets, and eddy mixing in the Southern Ocean. *JMR*, **68**, 479–502.

Marshall, J., A. Adcroft, C. Hill, L. Perelman, and C. Heisey, 1997a: A finite-volume, incompressible navier stokes model for studies of the ocean on parallel computers. *J. Geophys. Res.*, **102**, 5753–5766.

Marshall, J., C. Hill, L. Perelman, and A. Adcroft, 1997b: Hydrostatic, quasi-hydrostatic, and nonhydrostatic ocean modeling. *J. Geophys. Res.*, **102**, 5733–5752.

Marshall, J. and T. Radko, 2003: Residual-mean solutions for the ACC and its associated overturning circulation. *JPO*, **33**, 2341–2354.

Marshall, J., E. Shuckburgh, H. Jones, and C. Hill, 2006: Estimates and implications of surface eddy diffusivity in the Southern Ocean derived from tracer transport. *Journal of Physical Oceanography*, **36**, 1806–1821.

Marshall, J. and K. Speer, 2012: Closure of the meridional overturning circulation through southern ocean upwelling. *Nat. Geosci.*, **5**, 171–180, doi:10.1038/ngeo1391.

Mazloff, M., 2008: *The southern ocean meridional overturning circulation as diagnosed from an eddy permitting state estimate*. Ph.D. thesis, Massachusetts Institute of Technology.

Mazloff, M. R., R. Ferrari, and T. Schneider, 2013: The force balance of the Southern Ocean meridional overturning circulation. *Journal of Physical Oceanography*, **43**, 1193–1208.

Meredith, M. P., P. L. Woodworth, T. K. Chereskin, D. P. Marshall, L. C. Allison, G. R. Bigg, K. Donohue, K. J. Heywood, and C. W. Hughes, 2011: Sustained monitoring of the Southern Ocean at Drake Passage: past achievements and future priorities. *Rev. Geophys.*, **49**, RG4005, doi:10.1029/2010RG000348.

MITgcm Group, 2011: Mitgcm user manual, available online at `http://dev.mitgcm.org/public/r2_manual/latest/online_documents/manual.html`.

Naveira Garabato, A. C., R. Ferrari, and K. L. Polzin, 2011: Eddy stirring in the Southern Ocean. *J. Geophys. Res.*, **116**, C09019, doi:10.1029/2010JC006818.

Nikurashin, M. and R. Ferrari, 2011: Global energy conversion rate from geostrophic flows into internal lee waves in the deep ocean. *Geophysical Research Letters*, **38**, L08610, doi:10.1029/2011GL046576.

Nikurashin, M., G. K. Vallis, and A. Adcroft, 2013: Routes to energy dissipation for geostrophic flows in the Southern Ocean. *Nat. Geosci.*, **6**, 48–51, doi:10.1038/NGEO1657.

Nowlin, W. D., J. S. Bottero, and R. D. Pillsbury, 1982: Observations of the principal tidal currents at Drake Passage. *J. Geophys. Res.*, **87**, 5752–5770.

Nowlin, W. D., S. J. Worley, and T. W. III, 1985: Methods for making point estimates of eddy heat flux as applied to the Antarctic Circumpolar Current. *J. Geophys. Res.*, **90**, 3305–3324.

Phillips, H. E. and S. R. Rintoul, 2000: Eddy variability and energetics from direct current measurements in the Antarctic Circumpolar Current south of Australia. *Journal of Physical Oceanography*, **30**, 3050–3076.

Pillsbury, R. D., T. Whitworth III, and W. D. Nowlin, Jr., 1979: Currents and temperatures as observed in Drake Passage during 1975. *Journal of Physical Oceanography*, **9**, 469–482.

Plumb, R. A., 1986: Three-dimensional propagation of transient quasi-geostrophic eddies and its relationship with the eddy forcing of the time-mean flow. *J. Atmos. Sci.*, **43**, 1657–1678.

Plumb, R. A. and R. Ferrari, 2005: Transformed Eulerian-mean theory. I: Nonquasigeostrophic theory for eddies on a zonal mean flow. *Journal of Physical Oceanography*, **35**, 165–174.

Prather, M., 1986: Numerical advection by conservation of second-order moments. *J. Geophys. Res.*, **91**, 6671–6681.

Rio, M. H., S. Guinehut, and G. Larnicol, 2011: New cnes-cls09 global mean dynamic topography computed from the combination of grace data, altimetry, and in situ measurements. *J. Geophys. Res.*, **116**, C07018, doi:10.1029/2010JC006505.

Russell, J. L., K. W. Dixon, A. Gnanadesikan, R. J. Stouffer, and J. R. Toggweiler, 2006: The southern hemisphere westerlies in a warming world: Propping open the door to the deep ocean. *J. Climate*, **19**, 6382–6390, doi:10.1175/JCLI3984.1.

Shapiro, R., 1970: Smoothing, filtering, and boundary effects. *Rev. Geophys.*, **8**, 359–387.

Simmons, A., S. Uppala, D. Dee, and S. Kobayashi, 2006: Era-interim: New ECMWF reanalysis products from 1989 onwards. *ECMWF Newsletter*, **110**, 25–35, available online at http://www.ecmwf.int/publications/newsletters/.

Smith, K. S. and J. Marshall, 2009: Evidence for enhanced eddy mixing at mid-depth in the Southern Ocean. *Journal of Physical Oceanography*, **39**, 1037–1050.

Smith, W. H. F. and D. T. Sandwell, 2004: Conventional bathymetry, bathymetry from space, and geodetic altimetry. *Oceanography*, **17**, 8–23.

Speer, K., S. R. Rintoul, and B. Sloyan, 2000: The diabatic Deacon cell. *JPO*, **30**, 3212–3222.

Stammer, D., 1998: On eddy characteristics, eddy transports, and mean flow properties. *Journal of Physical Oceanography*, **28**, 727–739.

Taylor, G. I., 1921: Diffusion by continuous movements. *Proc. London Math. Soc.*, **20**, 196–212.

Treguier, A. M., 1999: Evaluating eddy mixing coefficients from eddy-resolving ocean models: A case study. *J. Marine Res.*, **57**, 89–108.

Tulloch, R. T., J. C. Marshall, C. Hill, and K. S. Smith, 2011: Scales, growth rates and spectral fluxes of baroclinic instability in the ocean. *Journal of Physical Oceanography*, **41**, 1057–1076, doi:10.1175/2011JPO4404.1.

Young, W. R., 1981: *The vertical structure of the wind-driven circulation*. Ph.D. thesis, Massachusetts Institute of Technology.

Zoubir, A. and B. Boashash, 1998: The bootstrap: Signal processing applications. *IEEE Transactions on Signal Processing*, **15**, 55–76.

Table 1: Brief information about the DIMES Cruises.

Cruise Code	Vessel	Cruise date	Days after release
US1	*R/V Roger Revelle*	22 Jan to 18 Feb 2009	0
US2	*R/V Thomas G. Thompson*	16 Jan to 23 Feb 2010	366
UK2	*RRS James Cook*	7 Dec to 5 Jan 2011	687
UK2.5	*RRS James Clark Ross*	11–25 Apr 2011	797
US3	*R/V Laurence M. Gould*	13–18 Aug 2011	917

Table 2: Observed estimates of the average rate of dispersion of the DIMES tracer over the first year on the US2 cruise track ($\sigma^2/2t$ at t=1 year in m^2s^{-1}). The 95% confidence intervals are determined using bootstrapping. The first three lines report estimates using three different methods to estimate $\sigma^2(1year)$ in both latitude and streamline coordinates (see Section 4.1 and Appendix A). The last two rows report our best estimate of the diffusivity obtained by multiplying the first two rows by a model derived factor that accounts for the incomplete tracer sampling during the US2 cruise (see Section 4.3). Bins of 1/2° width span from 65°S to 53°S in latitude coordinates, and from -1.75×10^4 m^2s^{-1} to 8 × 10^4 m^2s^{-1} in streamfunction coordinates.

Method	Latitude coordinates (y)	Stream coordinates (ψ)
Second moment	407 (323–495)	391 (227–558)
Binned second moment	524 (254–847)	476 (179–890)
Gaussian least-squares fit	708 (358–840)	665 (251–930)
Extrap. second moment	709±257	776± 436
Extrap. binned second moment	648±428	664± 520

Table 3: Modeled estimates of average rate of dispersion of the tracer ensemble over the first year using three methods and two coordinate systems ($\sigma^2/2t$ at t=1 year in m^{2}s^{-1}). The mean value is based on the ensemble average tracer, while the upper and lower bounds (in brackets) are the maximum and minumum values from the 12 tracer release experiments. Estimates using the full tracer west of 75°W are in the top three rows and estimates using the subsampled tracer on the US2 grid are in the bottom three rows. Bins of 1/2° width span from 65°S to 53°S in latitude coordinates, and from -1.75×10^4 m^{2}s^{-1} to 8 × 10^4 m^{2}s^{-1} in streamfunction space.

Method	Latitude coordinates (y)	Stream coordinates (ψ)
Full Second moment	888 (719–966)	903 (739–998)
Full Binned second moment	887 (717–967)	905 (743–1001)
Full Binned and least-squares fit	941 (672–1062)	1056 (816–1238)
US2 Second moment	510 (349–652)	455 (327–663)
US2 Binned second moment	717 (503–989)	649 (459–768)
US2 Binned and least-squares fit	968 (495–1474)	875 (472–1324)

Table 4: Numerical parameters used in the Drake Patch simulation.

Parameter	Value
Vertical viscosity (m^2s^{-1})	5.66×10^{-4}
Leith harmonic viscosity factor	1
Leith biharmonic viscosity factor	1.2
Vertical diffusivity (T,S) (m^2s^{-1})	1×10^{-5}
Side boundary	Free slip
Bottom boundary	No slip
Quadratic bottom drag (s^{-2})	2.5×10^{-3}
Time step (s)	120
Horizontal grid spacing (degrees)	0.05
Shear instability critical Richardson number	0.358

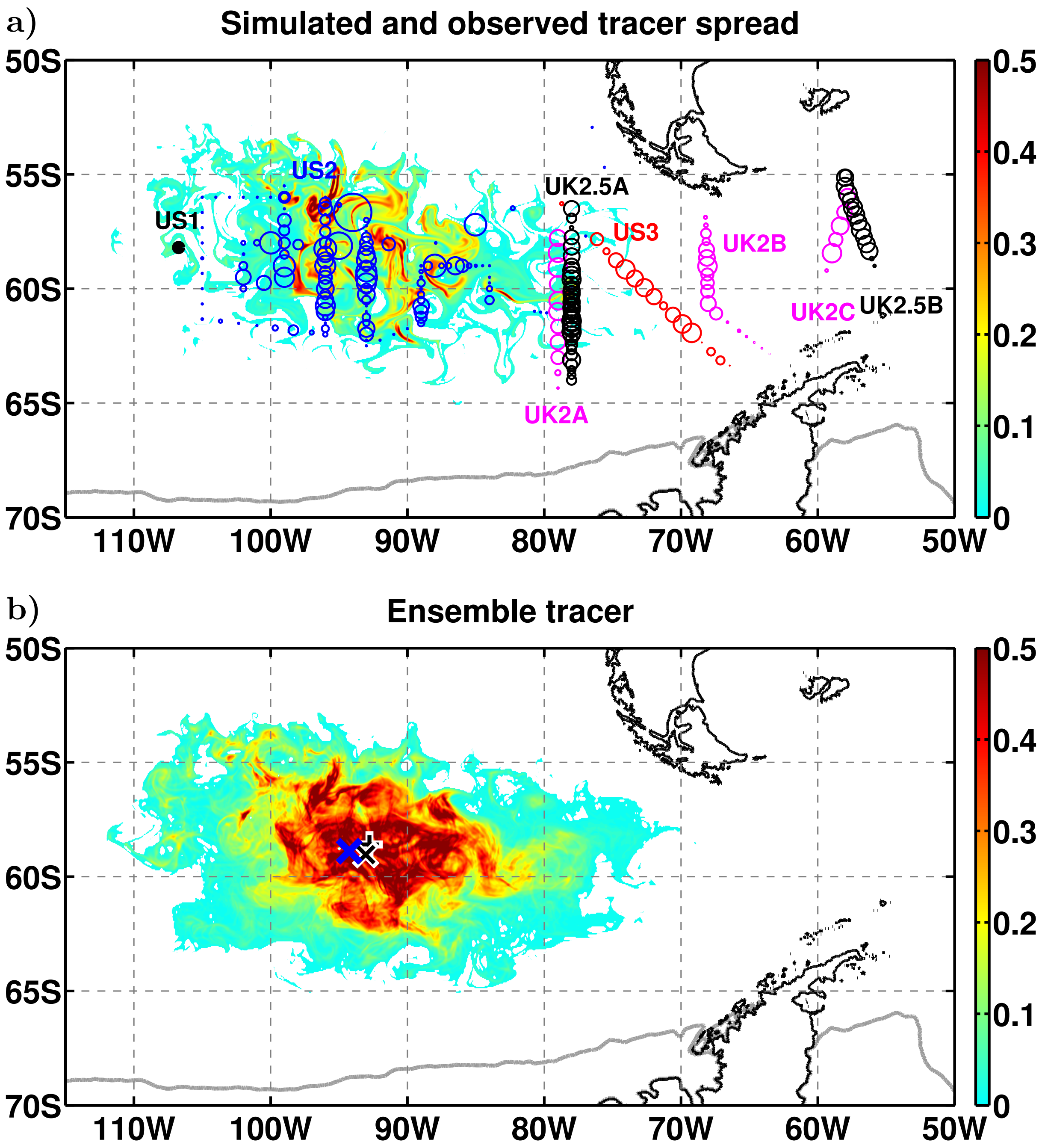

Figure 1: Caption next page.

Figure 1: (a) Map of DIMES tracer patch region showing the injection location (US1), and the column integrated tracer concentrations (circles) during subsequent cruises (US2, UK2, UK2.5, US3). The S2 two latitudinal transects at 96°W and 93°W are also referred to as 'US cruise 2A' and 'US cruise 2B'. The circle diameters are proportional to the tracer concentration. For each cruise the concentrations are normalized by the largest concentration found in that cruise. The contour plot in the background shows the column integrated concentration of a modeled tracer 365 days after release (cyan-to-red colormap). The modeled tracer concentration is also normalized by its maximum, and values less than 0.01 are shaded white. The climatological mean of the modeled sea ice extent is shown as a gray line. (b) Snapshot of the column integrated concentration from the ensemble average of 12 tracer release experiments 365 days after release. The blue 'x' marks the location of the center of mass of the DIMES tracer sampled on the US2 grid one year after release. The black 'x' is the location of the center of mass of the modeled ensemble tracer sampled only on the US2 grid, and the black '+' (beneath the black 'x') is the location of the emsemble tracer's center of mass based on the full tracer distribution.

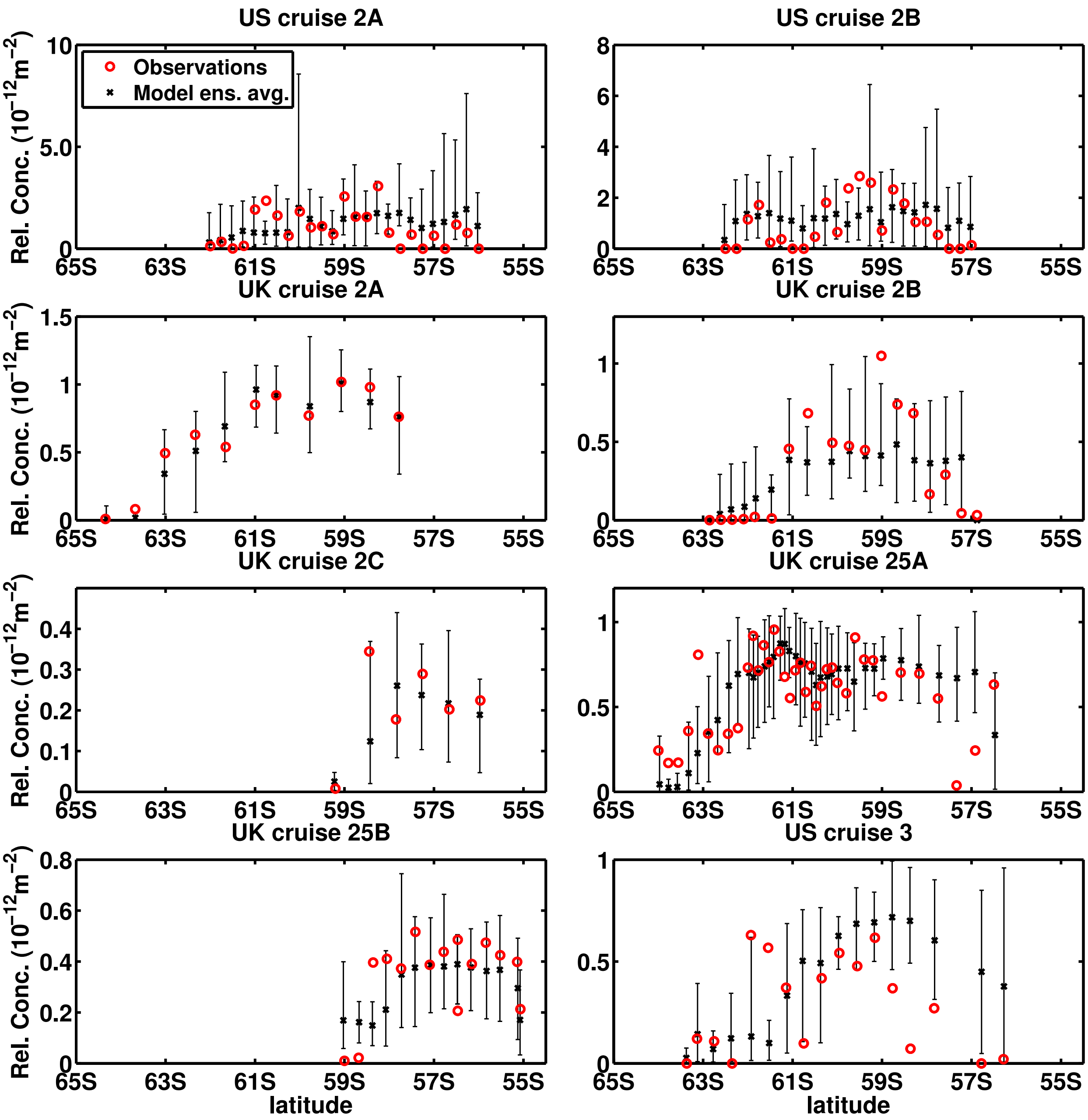

Figure 2: Observed (circles) and simulated (x's) column-integrated tracer concentrations relative to the total amount of tracer released (units are m^{-2}) measured at individual stations during the cruises listed in Table 1 and shown in Fig. 1. Only a subset of Cruise US2 is shown: US-2A is the latitudinal transect at 96° and US-2B is the latitudinal transect at 93°. The spread in the modeled ensemble mean concentrations, shown as thin black lines, is based on the maximum and minimum concentrations at each point of all 12 release experiments.

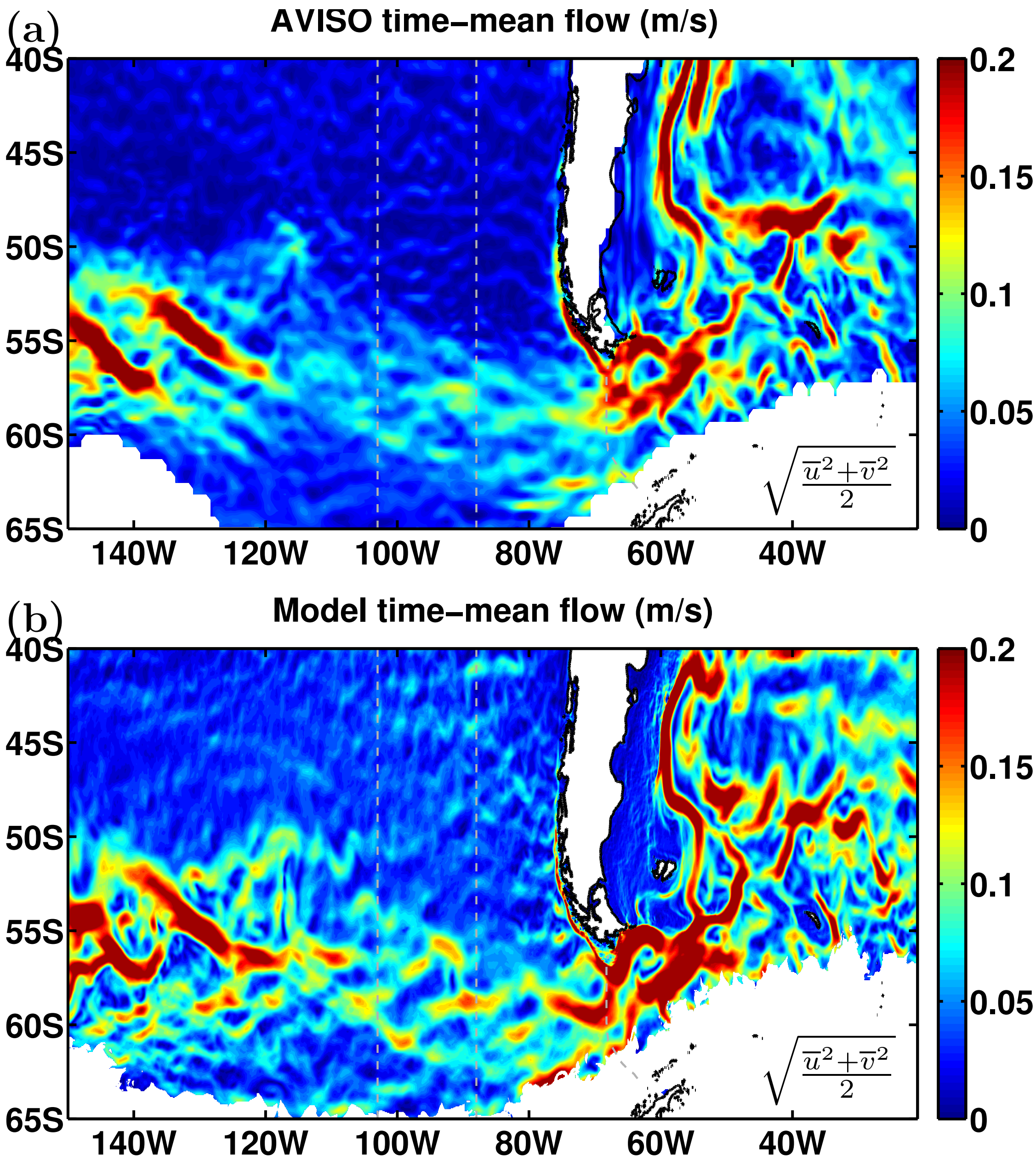

Figure 3: (a) Altimetry based (AVISO) time-mean geostrophic current speed averaged from 1993 to 2011. Regions around Antarctica where the AVISO data were sometimes missing during the averaging period are left white. (b) Modeled time mean current speed averaged over model integration years 6, 7 and 8. White regions around Antarctica indicate maximum sea ice extent over the 3 year period. The two faint dashed lines are the locations of WOCE and CLIVAR sections P18, P19, and A21 shown in Fig. 14.

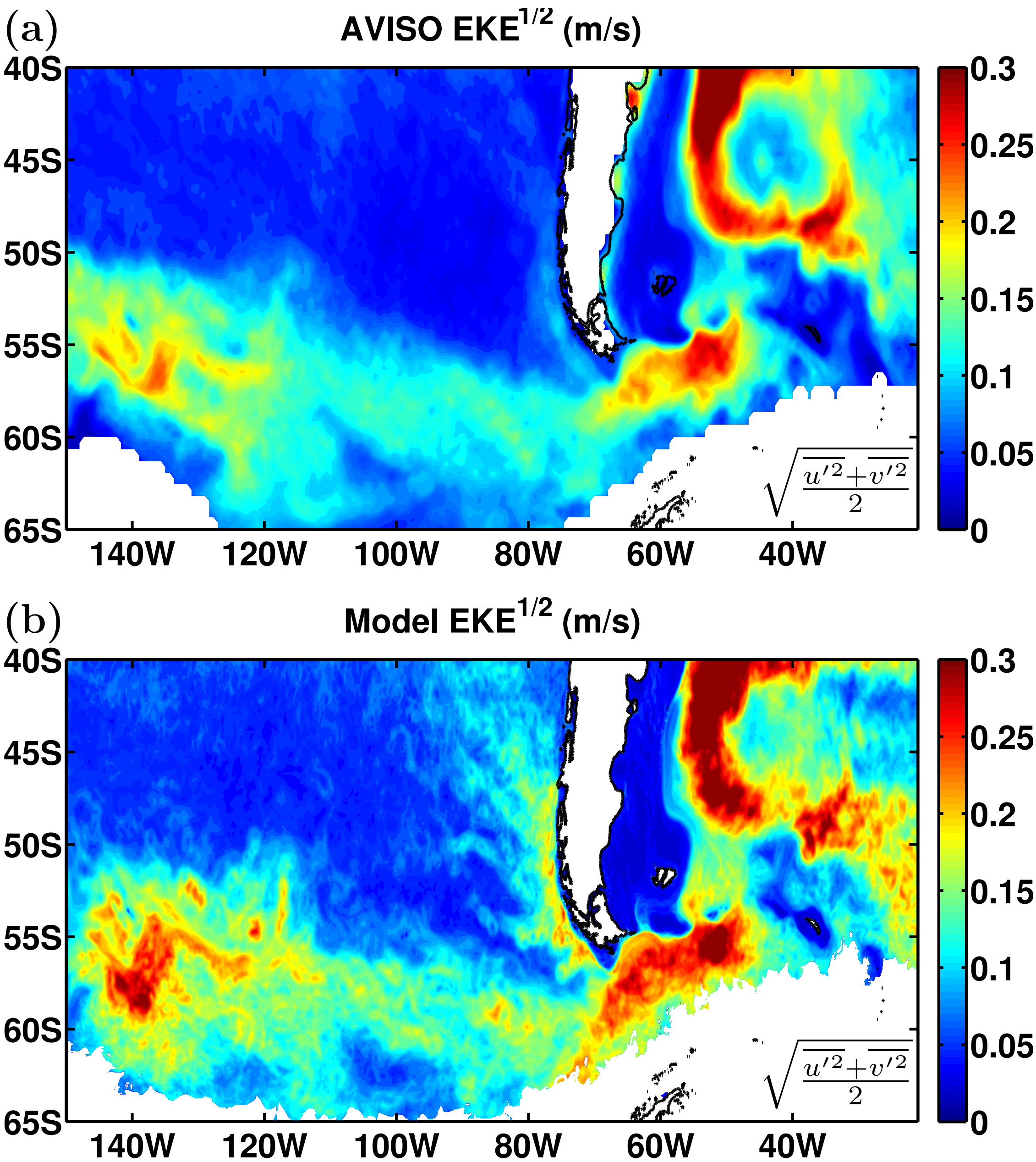

Figure 4: (a) AVISO geostrophic eddy current speeds ($\mathrm{EKE}^{1/2}$) and (b) modeled eddy current speeds. The EKE is defined as the temporal fluctuation about the averages shown in Fig. 3.

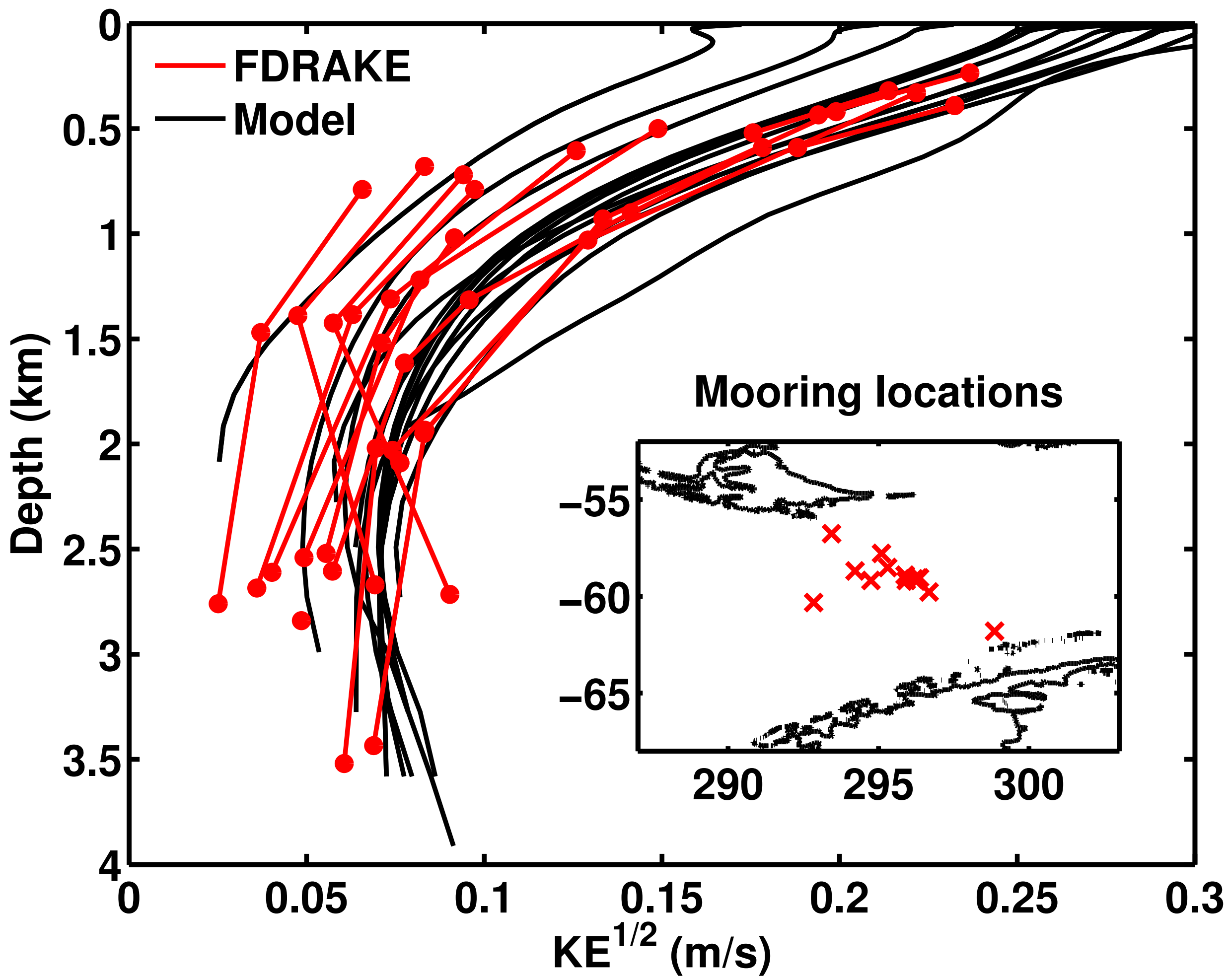

Figure 5: Comparison of simulated vertical structure of current speed ($KE^{1/2}$) (black lines) against FDRAKE mooring data from the late 1970's (red lines). The location of each FDRAKE mooring is plotted in the inset. The average length of the mooring data is 320 days. The black line with the largest EKE in the model is from the northernmost mooring location.

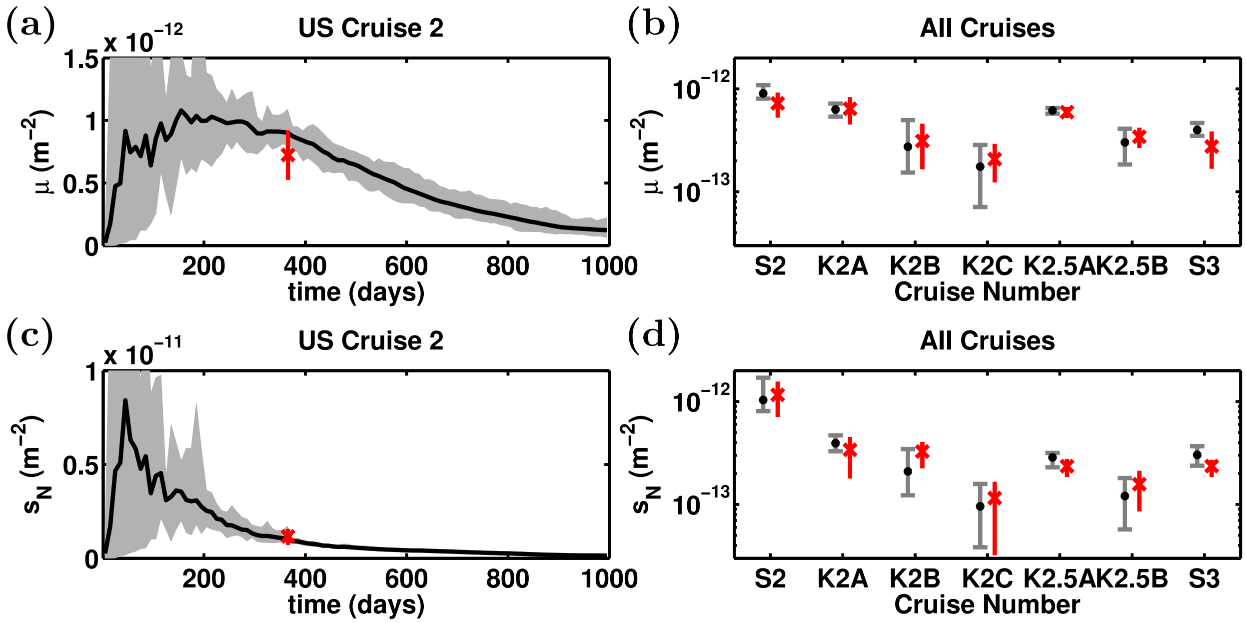

Figure 6: (a) Modeled average ($\mu = N^{-1}\sum c_i$) and (c) standard deviation ($s_N = \sqrt{(N-1)^{-1}\sum(c_i-\mu)^2}$) of the column integrated tracer concentration at the US2 cruise track locations versus time. The tracer concentrations are normalized by the total amount of tracer released, hence the units are m^{-2}. The red 'x' shows the observed tracer concentration from the DIMES US2 cruise, with the red line indicating a 95% confidence interval using bootstrapping. Gray shading indicates the minimum and maximum values from the 12 tracer releases from the ensemble. (b) and (d) show the same means and standard deviations, but at the times listed in Table 1 for the 4 DIMES cruises. The UK2 and UK2.5 cruises have been split into individual transects from west to east (K2A, K2B, K2C and K2.5A and K2.5B respectively. US2 and US3 transects are represented by S2 and S3. Notice that we used a logarithmic scale in these two panels, because the concentrations drop substantially two to three years after injection.

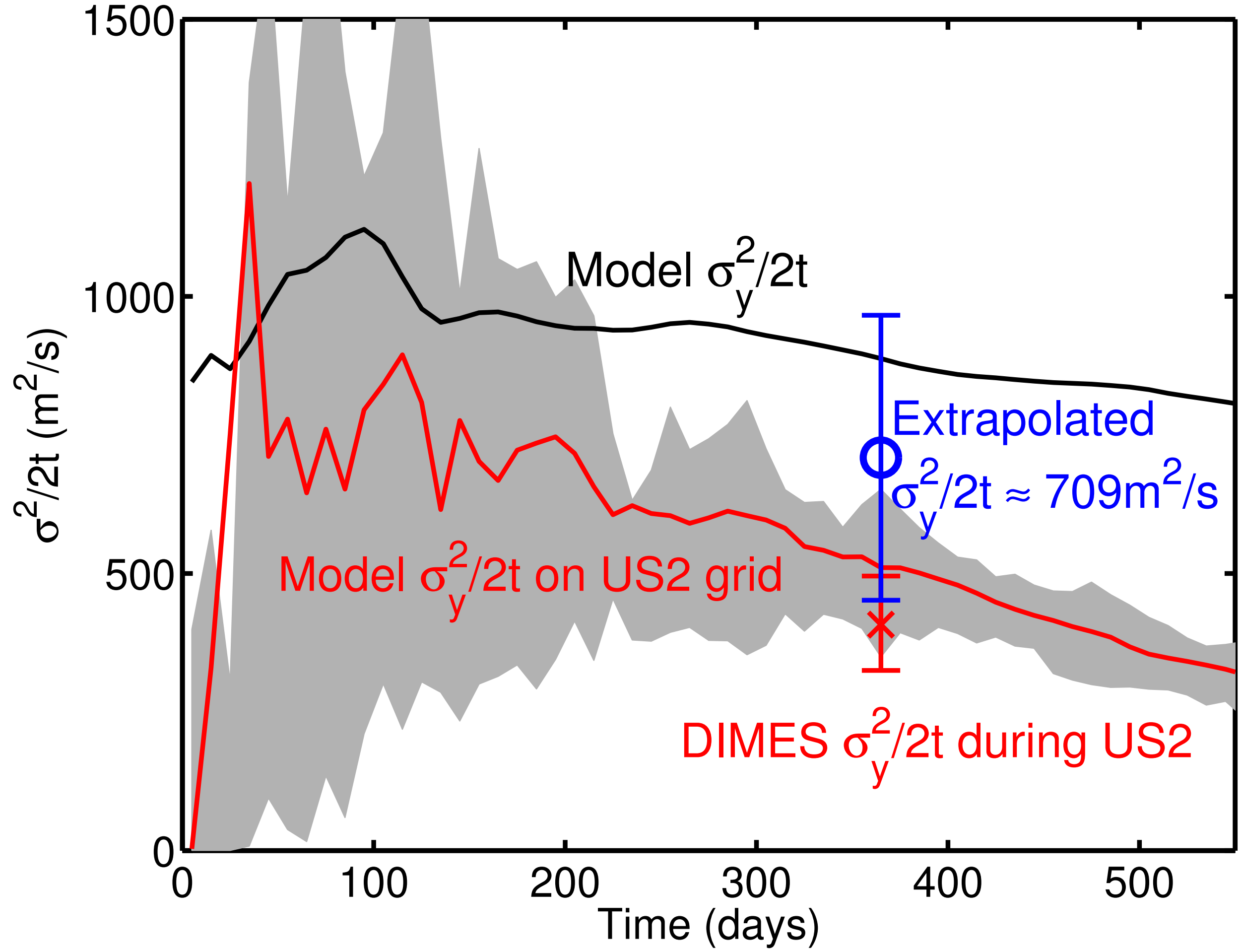

Figure 7: Comparison of the average rate of dispersion using: the full model ensemble average tracer $\sigma_y^2|_{model\ full}/2t$ (black line), the ensemble average tracer subsampled on the US2 cruise stations $\sigma_y^2|_{model\ US2}/2t$ (red line) and the observed DIMES tracer during US2 $\sigma_y^2|_{DIMES}/2t$ (red 'x'). The gray shading indicates the minima and maxima from the 12 release experiments. A 95% confidence interval on the DIMES tracer is estimated using bootstrapping. The blue circle and the blue error bar indicates the extrapolated estimate of the average rate of dispersion over the first year of the DIMES tracer using Eqs. 8 and 9.

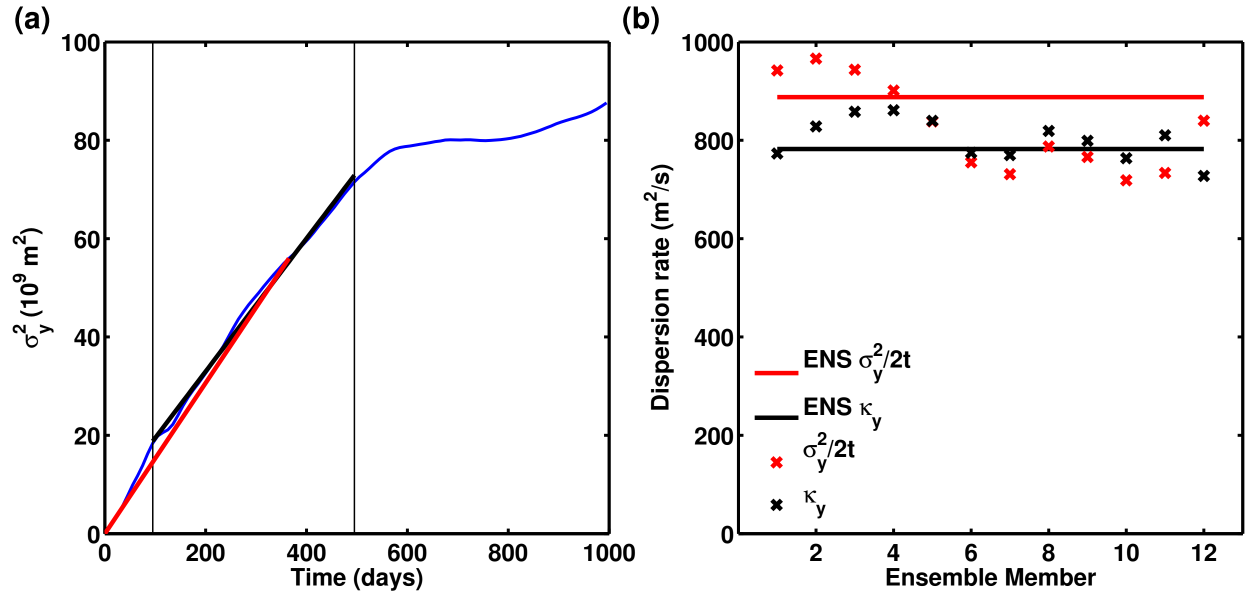

Figure 8: (a) Dispersion σ_y^2 of the ensemble mean tracer in the simulation versus time (blue line). The red line marks the average dispersion in the first year after release, with slope $\sigma_y^2(t)/2t$ where $t = 365$, and the black line marks a least-squares fit to the dispersion from $t = 100$ d to $t = 500$ d. (b) The slopes of the red and black lines in (a) are plotted in (b) as solid red and black lines. The slopes of each of the 12 tracer release experiments in the ensemble are plotted as red and black x's.

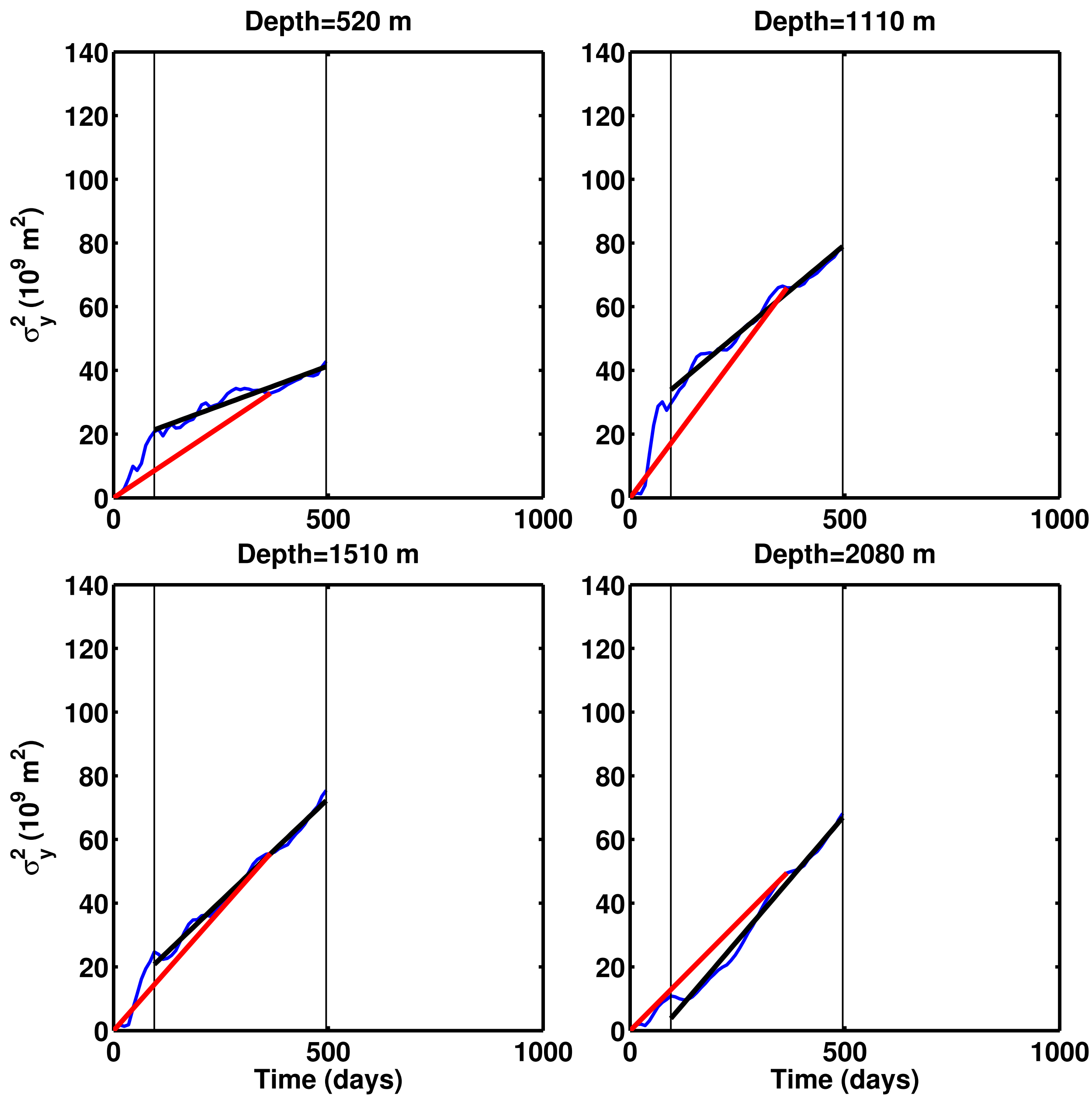

Figure 9: Dispersion σ_y^2 from model tracers released at depths near 500 m, 1 km, 1.5 km, and 2 km (blue lines). The red lines are the average dispersion over the first year and the black lines are the least-squares fit dispersion between $t = 100$ d and $t = 500$ d as in Fig. 8.

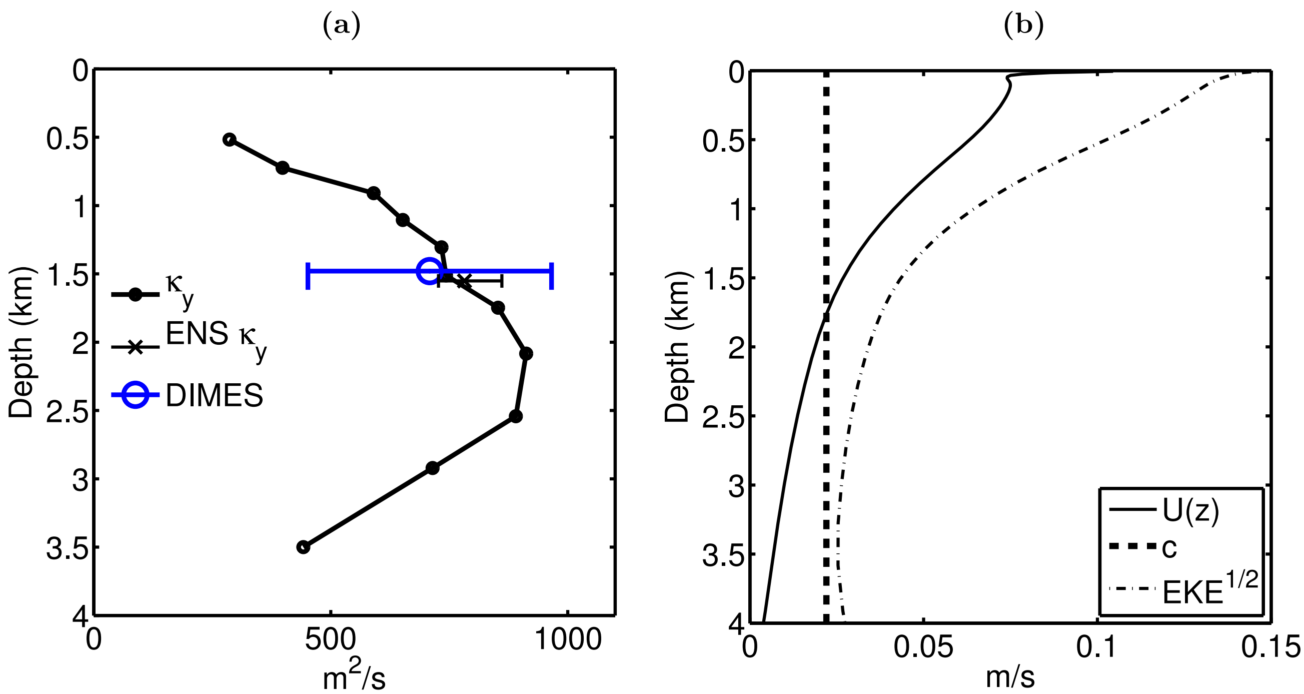

Figure 10: (a) Estimates of the vertical structure of the isopycnal eddy diffusivity upstream of 75°W at various depths. The eddy diffusivity is estimated as the least-squares fit dispersion between day 100 and day 500 (see Fig. 9). The estimates from the ensemble average tracer released at 1500 m is indicated as a black 'x' with the error bar showing the minimum and maximum values from the 12 release experiments. The blue circle and line are the observational estimate with its uncertainty. (b) Model estimate of the mean flow, $U(z)$, eddy phase speed, c, and $EKE^{1/2}$, all averaged between 61°S and 56°S and between 110°W and 80°W.

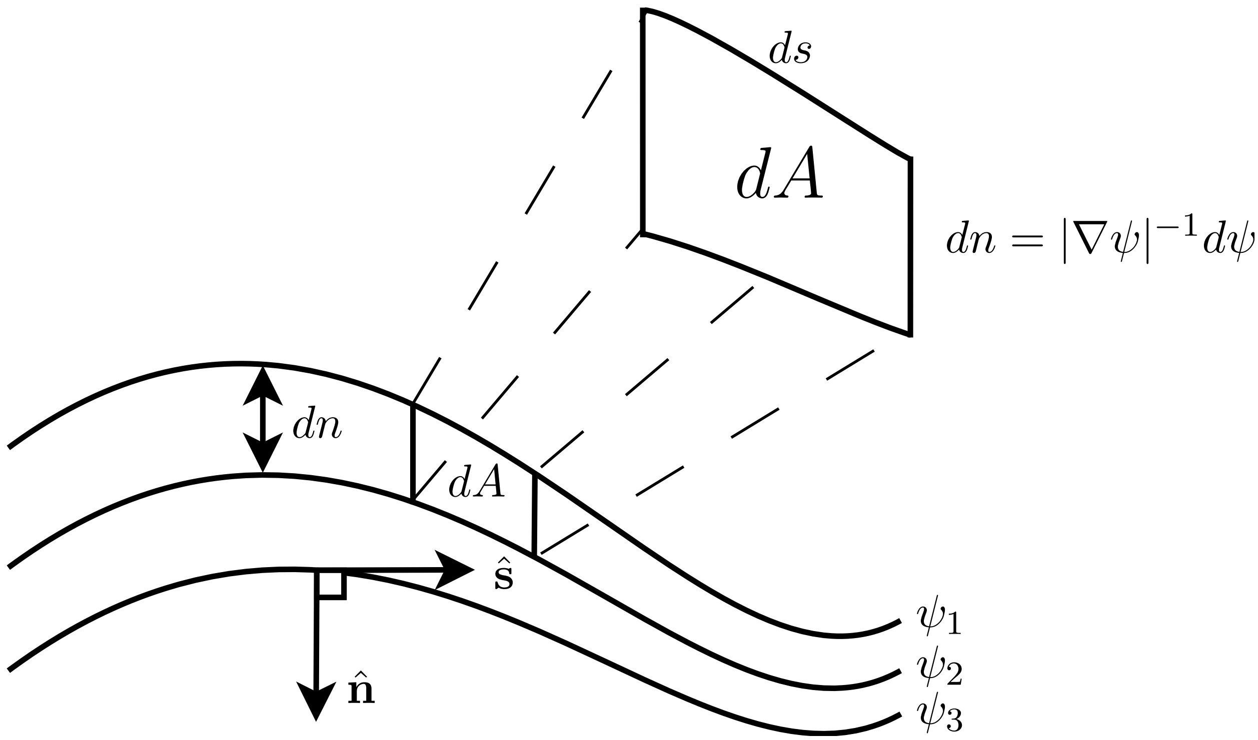

Figure 11: Streamline coordinate system. The s coordinate is along streamlines, the n coordinate is normal to it. The area of the patch dA in streamline coordinates is indicated.

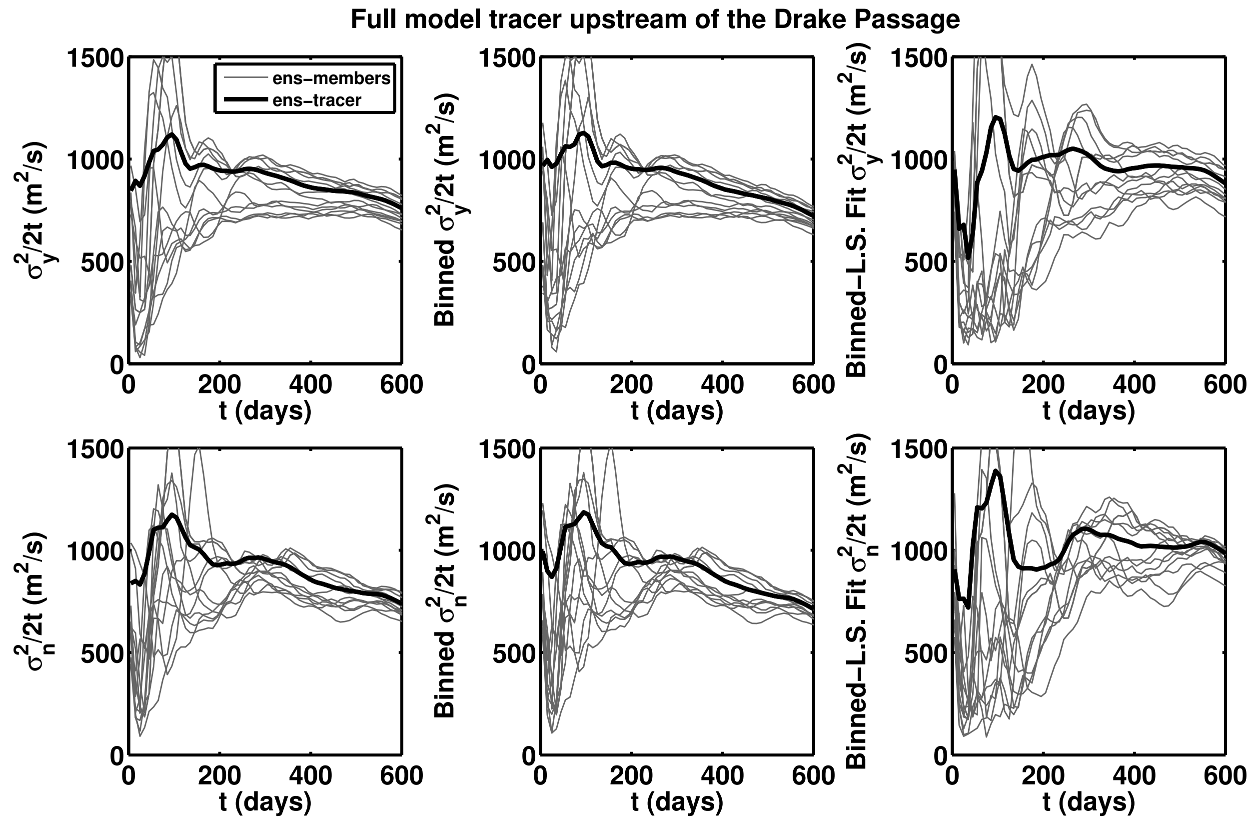

Figure 12: Three model based estimates (left to right) of eddy diffusivity at 1500 m in latitude coordinates (top) and streamline coordinates (bottom). The eddy diffusivity is determined as the growth rate of the second moment of the tracer concentration. The three estimates of the second moment in latitude coordinates are: the second moment averaged over the whole area occupied by the tracer $\sigma_y^2 =< y^2 c > / < c >$ (left), meridional binning followed by second moment $\sigma_y^2 = \sum y^2 \int c \; dx / \sum \int c \; dx$ (middle), and meridional binning followed by a least-squares fit to a Gaussian using gradient descent (right). The thick black line are estimated based on the ensemble average tracer $\overline{c}$, while the grey lines are estimates based on the 12 individual tracer release experiments.

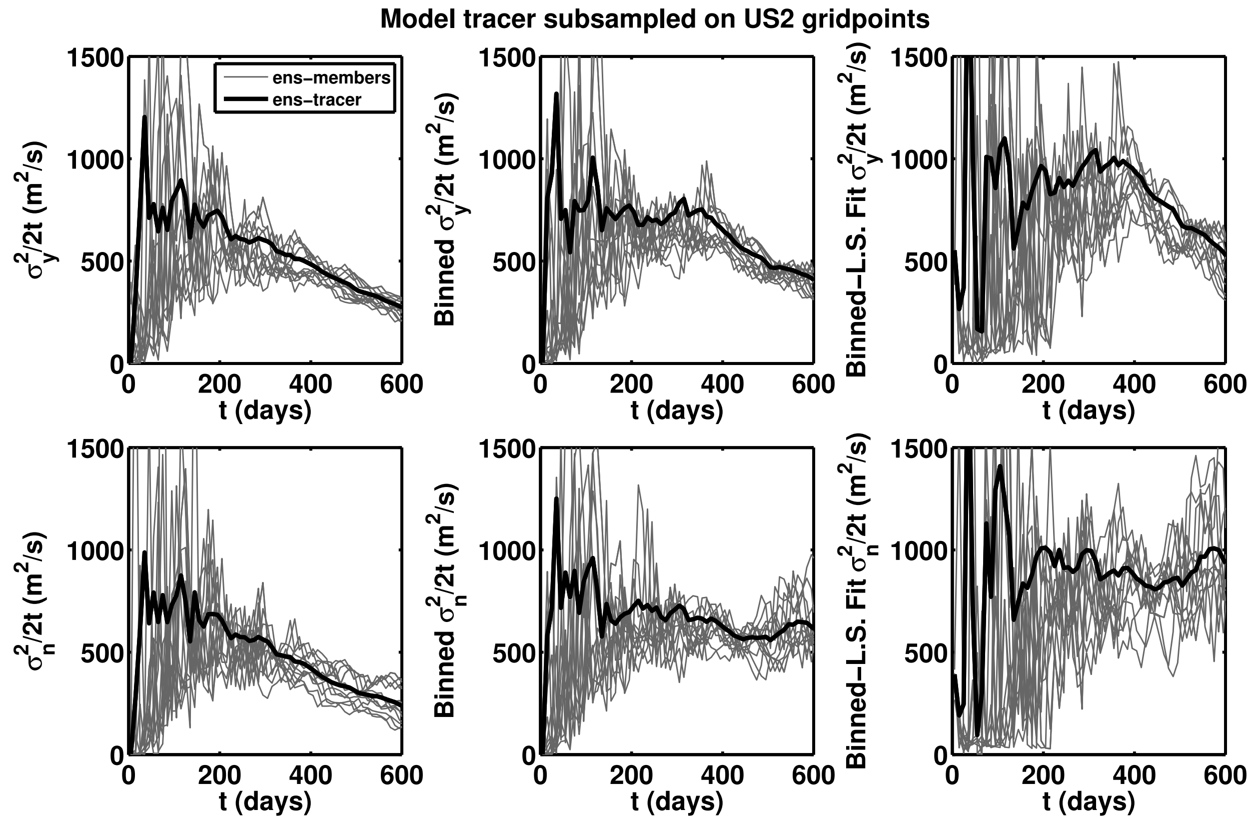

Figure 13: Three estimates (left to right) of diffusivity at 1500 m in the model using tracer subsampled on the US2 station locations, in latitude coordinates (top) and streamline coordinates (bottom). The eddy diffusivity is determined as the growth rate of the second moment of the tracer concentration. The three estimates of the second moment (in latitude coordinates) are: the second moment $\sigma_y^2 = \sum_i y_i^2 \bar{c}_i / \sum_i \bar{c}_i$ (left); the meridionally binned second moment $\sigma_y^2 = \sum_j \left(y_j^2 \sum_i \bar{c}_i \right) / \sum_i \left(\sum_i \bar{c}_i \right)$ where j is a sum over bins and i is a sum over points within each bin (middle); the least-squares fit to a Gaussian after binning meridionally.

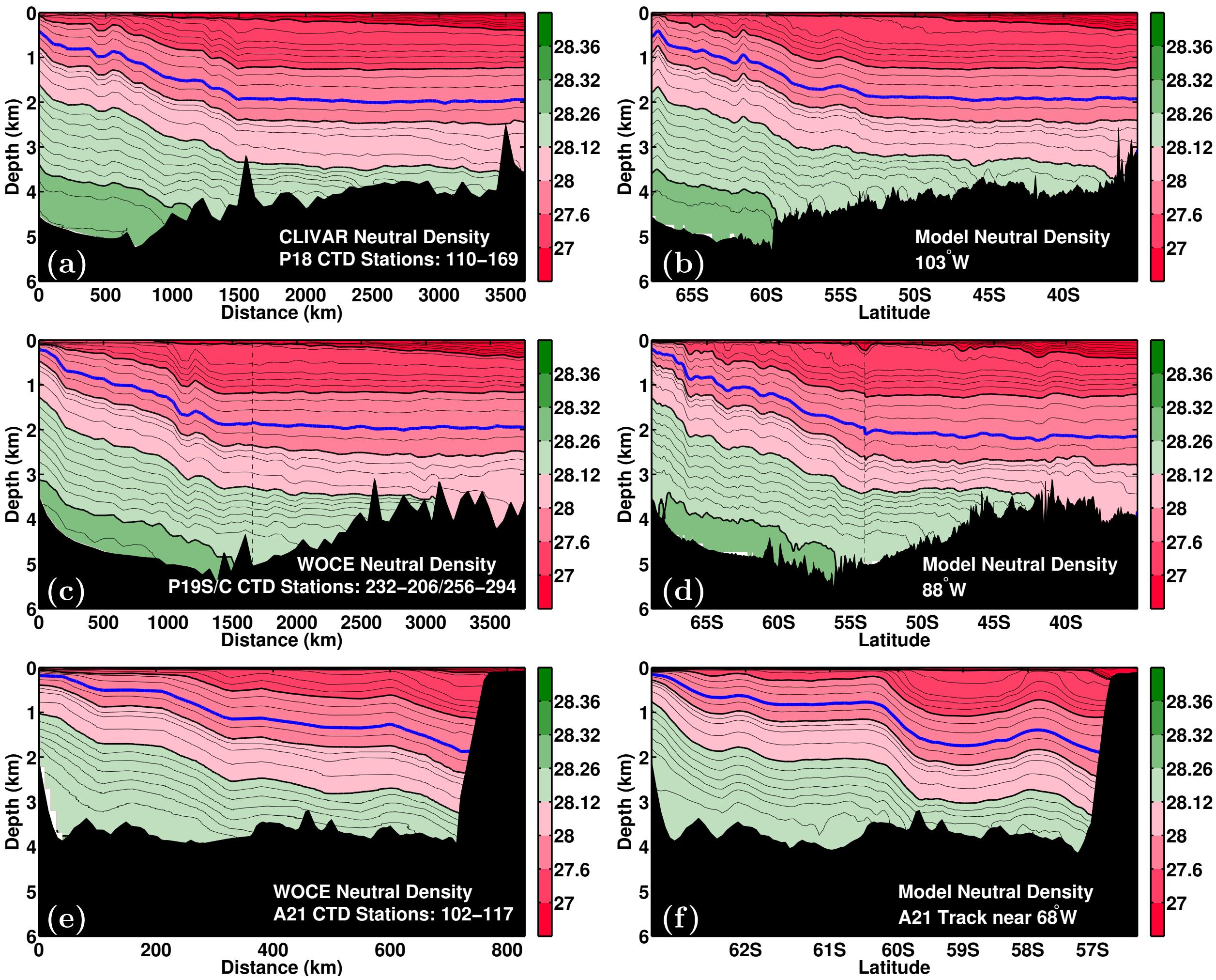

Figure 14: Comparison of neutral density from (left) WOCE and CLIVAR sections P18 (top), P19 (middle), and A21 (bottom) with (right) the Drake Patch model at 103°W (top), 88°W (middle), and near (68°W, 61°S) following A21 (bottom). The CTD profiles were collected December to January 2007-2008 (P18), December to March 1992-1993 (P19) and late January 1990 (A21), and were plotted as a section using Delaunay triangulation with cubic interpolation. The CTD sections were downloaded from the electronic atlas at `http://cchdo.ucsd.edu/data/co2clivar/pacific`, subdirectories `a21`, `p17`, `p18`, and `p19`. The modeled sections are snapshots on January 19 of the 6th year of integration for P18, the southern part of P19 and A21, and February 18 for the northern part of P19. The blue lines track the neutral density surface 27.9 kg m^{-3} along which the DIMES tracer was injected.

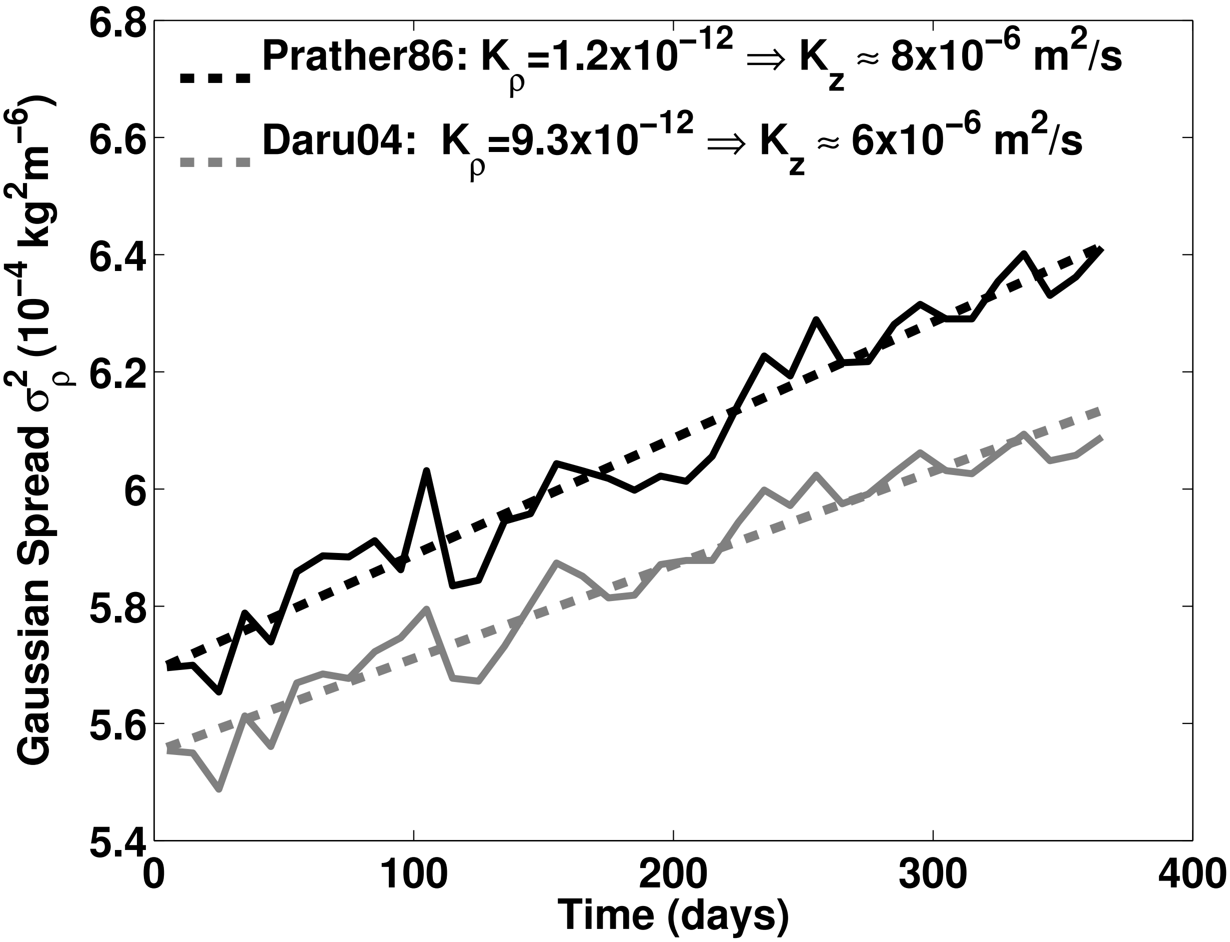

Figure 15: Evolution of the variance of the tracer spread in density space for a tracer that was injected with a Gaussian concentration in the vertical, advected by advection schemes of Prather (1986) and Daru and Tenaud (2004). The squared half-width $\sigma_\rho(t)^2$ (indicated as continuous lines) is for a Gaussian fitted to the vertical profile of the tracer after integration along neutral density surfaces. A diapycnal eddy diffusivity is estimated as half the growth rate of $\sigma_\rho(t)^2$ (dashed lines). Converting into z-coordinates both schemes imply diapycnal mixing $K^z < 10^{-5}$ m^{2}s^{-1}.

Figure Captions

Fig. 1: (a) Map of DIMES tracer patch region showing the injection location (US1), and the column integrated tracer concentrations (circles) during subsequent cruises (US2, UK2, UK2.5, US3). The S2 two latitudinal transects at 96°W and 93°W are also referred to as 'US cruise 2A' and 'US cruise 2B'. The circle diameters are proportional to the tracer concentration. For each cruise the concentrations are normalized by the largest concentration found in that cruise. The contour plot in the background shows the column integrated concentration of a modeled tracer 365 days after release (cyan-to-red colormap). The modeled tracer concentration is also normalized by its maximum, and values less than 0.01 are shaded white. The climatological mean of the modeled sea ice extent is shown as a gray line. (b) Snapshot of the column integrated concentration from the ensemble average of 12 tracer release experiments 365 days after release. The blue 'x' marks the location of the center of mass of the DIMES tracer sampled on the US2 grid one year after release. The black 'x' is the location of the center of mass of the modeled ensemble tracer sampled only on the US2 grid, and the black '+' (beneath the black 'x') is the location of the emsemble tracer's center of mass based on the full tracer distribution.

Fig. 2: Observed (circles) and simulated (x's) column-integrated tracer concentrations relative to the total amount of tracer released (units are m^{-2}) measured at individual stations during the cruises listed in Table 1 and shown in Fig. 1. Only a subset of Cruise US2 is shown: US-2A is the latitudinal transect at 96° and US-2B is the latitudinal transect at 93°. The spread in the modeled ensemble mean concentrations, shown as thin black lines, is based

on the maximum and minimum concentrations at each point of all 12 release experiments.

Fig. 3: (a) Altimetry based (AVISO) time-mean geostrophic current speed averaged from 1993 to 2011. Regions around Antarctica where the AVISO data were sometimes missing during the averaging period are left white. (b) Modeled time mean current speed averaged over model integration years 6, 7 and 8. White regions around Antarctica indicate maximum sea ice extent over the 3 year period. The two faint dashed lines are the locations of WOCE and CLIVAR sections P18, P19, and A21 shown in Fig. 14.

Fig. 4: (a) AVISO geostrophic eddy current speeds ($\mathrm{EKE}^{1/2}$) and (b) modeled eddy current speeds. The EKE is defined as the temporal fluctuation about the averages shown in Fig. 3.

Fig. 5: Comparison of simulated vertical structure of current speed ($\mathrm{KE}^{1/2}$) (black lines) against FDRAKE mooring data from the late 1970's (red lines). The location of each FDRAKE mooring is plotted in the inset. The average length of the mooring data is 320 days. The black line with the largest EKE in the model is from the northernmost mooring location.

Fig. 6: (a) Modeled average ($\mu = N^{-1}\sum c_i$) and (c) standard deviation ($s_N = \sqrt{(N-1)^{-1}\sum(c_i-\mu)^2}$) of the column integrated tracer concentration at the US2 cruise track locations versus time. The tracer concentrations are normalized by the total amount of tracer released, hence the units are m^{-2}. The red 'x' shows the observed tracer concentration from the DIMES US2 cruise, with the red line indicating a 95% confidence interval using bootstrapping. Gray

shading indicates the minimum and maximum values from the 12 tracer releases from the ensemble. (b) and (d) show the same means and standard deviations, but at the times listed in Table 1 for the 4 DIMES cruises. The UK2 and UK2.5 cruises have been split into individual transects from west to east (K2A, K2B, K2C and K2.5A and K2.5B respectively. US2 and US3 transects are represented by S2 and S3. Notice that we used a logarithmic scale in these two panels, because the concentrations drop substantially two to three years after injection.

Fig. 7: Comparison of the average rate of dispersion using: the full model ensemble average tracer $\sigma_y^2|_{model\ full}/2t$ (black line), the ensemble average tracer subsampled on the US2 cruise stations $\sigma_y^2|_{model\ US2}/2t$ (red line) and the observed DIMES tracer during US2 $\sigma_y^2|_{DIMES}/2t$ (red 'x'). The gray shading indicates the minima and maxima from the 12 release experiments. A 95% confidence interval on the DIMES tracer is estimated using bootstrapping. The blue circle and the blue error bar indicates the extrapolated estimate of the average rate of dispersion over the first year of the DIMES tracer using Eqs. 8 and 9.

Fig. 8: (a) Dispersion σ_y^2 of the ensemble mean tracer in the simulation versus time (blue line). The red line marks the average dispersion in the first year after release, with slope $\sigma_y^2(t)/2t$ where $t = 365$, and the black line marks a least-squares fit to the dispersion from $t = 100$ d to $t = 500$ d. (b) The slopes of the red and black lines in (a) are plotted in (b) as solid red and black lines. The slopes of each of the 12 tracer release experiments in the ensemble are plotted as red and black x's.

Fig. 9: Dispersion σ_y^2 from model tracers released at depths near 500 m, 1 km, 1.5 km, and 2 km (blue lines). The red lines are the average dispersion over the first year and the black lines are the least-squares fit dispersion between $t = 100$ d and $t = 500$ d as in Fig. 8.

Fig. 10: (a) Estimates of the vertical structure of the isopycnal eddy diffusivity upstream of 75°W at various depths. The eddy diffusivity is estimated as the least-squares fit dispersion between day 100 and day 500 (see Fig. 9). The estimates from the ensemble average tracer released at 1500 m is indicated as a black 'x' with the error bar showing the minimum and maximum values from the 12 release experiments. The blue circle and line are the observational estimate with its uncertainty. (b) Model estimate of the mean flow, $U(z)$, eddy phase speed, c, and $EKE^{1/2}$, all averaged between 61°S and 56°S and between 110°W and 80°W.

Fig. 11: Streamline coordinate system. The s coordinate is along streamlines, the n coordinate is normal to it. The area of the patch dA in streamline coordinates is indicated.

Fig. 12: Three model based estimates (left to right) of eddy diffusivity at 1500 m in latitude coordinates (top) and streamline coordinates (bottom). The eddy diffusivity is determined as the growth rate of the second moment of the tracer concentration. The three estimates of the second moment in latitude coordinates are: the second moment averaged over the whole area occupied by the tracer $\sigma_y^2 =< y^2 c > / < c >$ (left), meridional binning followed by second moment $\sigma_y^2 = \sum y^2 \int c \, dx / \sum \int c \, dx$ (middle), and meridional binning followed by a least-squares fit to a Gaussian using gradient descent (right). The thick black line are

estimated based on the ensemble average tracer $\overline{c}$, while the grey lines are estimates based on the 12 individual tracer release experiments.

Fig. 13: Three estimates (left to right) of diffusivity at 1500 m in the model using tracer subsampled on the US2 station locations, in latitude coordinates (top) and streamline coordinates (bottom). The eddy diffusivity is determined as the growth rate of the second moment of the tracer concentration. The three estimates of the second moment (in latitude coordinates) are: the second moment $\sigma_y^2 = \sum_i y_i^2 \overline{c}_i / \sum_i \overline{c}_i$ (left); the meridionally binned second moment $\sigma_y^2 = \sum_j \left(y_j^2 \sum_i \overline{c}_i \right) / \sum_i \left(\sum_i \overline{c}_i \right)$ where j is a sum over bins and i is a sum over points within each bin (middle); the least-squares fit to a Gaussian after binning meridionally.

Fig. 14: Comparison of neutral density from (left) WOCE and CLIVAR sections P18 (top), P19 (middle), and A21 (bottom) with (right) the Drake Patch model at 103°W (top), 88°W (middle), and near (68°W, 61°S) following A21 (bottom). The CTD profiles were collected December to January 2007-2008 (P18), December to March 1992-1993 (P19) and late January 1990 (A21), and were plotted as a section using Delaunay triangulation with cubic interpolation. The CTD sections were downloaded from the electronic atlas at `http://cchdo.ucsd.edu/data/co2clivar/pacific`, subdirectories `a21`, `p17`, `p18`, and `p19`. The modeled sections are snapshots on January 19 of the 6th year of integration for P18, the southern part of P19 and A21, and February 18 for the northern part of P19. The blue lines track the neutral density surface 27.9 kg m^{-3} along which the DIMES tracer was injected.

Fig. 15: Evolution of the variance of the tracer spread in density space for a tracer that

was injected with a Gaussian concentration in the vertical, advected by advection schemes of Prather (1986) and Daru and Tenaud (2004). The squared half-width $\sigma_\rho(t)^2$ (indicated as continuous lines) is for a Gaussian fitted to the vertical profile of the tracer after integration along neutral density surfaces. A diapycnal eddy diffusivity is estimated as half the growth rate of $\sigma_\rho(t)^2$ (dashed lines). Converting into z-coordinates both schemes imply diapycnal mixing $K^z < 10^{-5}$ m^{2}s^{-1}.